Since January 2020 Elsevier has created a COVID-19 resource centre with free information in English and Mandarin on the novel coronavirus COVID-19. The COVID-19 resource centre is hosted on Elsevier Connect, the company's public news and information website.

Science of the Total Environment 808 (2022) 152191

Contents lists available at ScienceDirect

Science of the Total Environment

journal homepage: www.elsevier.com/locate/scitotenv

Evolution of organic carbon during COVID-19 lockdown period: Possible contribution of nocturnal chemistry

Zemin Feng [a], Feixue Zheng [a], Yongchun Liu [a,d,*], Xiaolong Fan [a], Chao Yan [c], Yusheng Zhang [a], Kaspar R. Daellenbach [c], Federico Bianchi [c], Tuukka Petäjä [c], Markku Kulmala [a,c], Xiaolei Bao [b,e,**]

[a] Aerosol and Haze Laboratory, Advanced Innovation Center for Soft Matter Science and Engineering, Beijing University of Chemical Technology, Beijing 100029, China
[b] Hebei Provincial Academy of Environmental Sciences, Shijiazhuang 050037, China
[c] Institute for Atmospheric and Earth System Research/Physics, Faculty of Science, University of Helsinki, Finland
[d] College of Chemistry and Chemical Engineering, China West Normal University, Nanchong 637002, China
[e] Hebei Chemical & Pharmaceutical College, Shijiazhuang 050026, China

HIGHLIGHTS

- Higher concentration of SOC was observed during the lockdown period than the normal period.
- Nocturnal chemistry related to NO_3 radicals contributed to increase of SOC.
- The southeast regions of the NCP contributed more to SOC during the lockdown period than the normal period.

GRAPHICAL ABSTRACT

Potential source of SOC during COVID-19 pandemic.

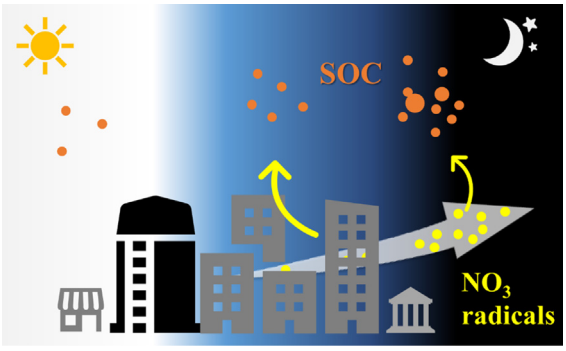

ARTICLE INFO

Article history:
Received 25 September 2021
Received in revised form 15 November 2021
Accepted 1 December 2021
Available online 5 December 2021

Editor: Jianmin Chen

Keywords:
Carbonaceous aerosol
Secondary organic carbon
NO_3 radicals
Nocturnal chemistry

ABSTRACT

Carbonaceous aerosol is one of the main components of atmospheric particulate matter, which is of great significance due to its role in climate change, earth's radiation balance, visibility, and human health. In this work, carbonaceous aerosols were measured in Shijiazhuang and Beijing using the OC/EC analyzer from December 1, 2019 to March 15, 2020, which covered the Coronavirus Disease 2019 (COVID-19) pandemic. The observed results show that the gas-phase pollutants, such as NO, NO_2, and aerosol-phase pollutants (Primary Organic Compounds, POC) from anthropogenic emissions, were significantly reduced during the lockdown period due to limited human activities in North China Plain (NCP). However, the atmospheric oxidation capacity (Ox/CO) shows a significantly increase during the lockdown period. Meanwhile, additional sources of nighttime Secondary Organic Carbon (SOC), Secondary Organic Aerosol (SOA), and $b_{abs,\ BrC}$(370 nm) are observed and ascribed to the nocturnal chemistry related to NO_3 radical. The Potential Source Contribution Function (PSCF) analysis indicates that the southeast areas of the NCP region contributed more to the SOC during the lockdown period than the normal period. Our results highlight the importance of regional nocturnal chemistry in SOA formation.

* Correspondence to: Y. Liu, Aerosol and Haze Laboratory, Advanced Innovation Center for Soft Matter Science and Engineering, Beijing University of Chemical Technology, Beijing 100029, China.
** Correspondence to: X. Bao, Hebei Provincial Academy of Environmental Sciences, Shijiazhuang 050037, China.
E-mail addresses: liuyc@buct.edu.cn (Y. Liu), bxl5@163.com (X. Bao).

http://dx.doi.org/10.1016/j.scitotenv.2021.152191

1. Introduction

Over the past few decades, the poor air quality in China has attracted intensive attentions (Fan et al., 2021; Liu et al., 2020a; Wang et al., 2021b; Zong et al., 2021). To improve air quality, the Chinese government has implemented a series of strict emission control strategies, such as the Air Pollution Prevention and Control Action Plan in 2013 (Cai et al., 2017; Ge et al., 2021). As a consequence, particulate mass concentration with a diameter less than 2.5 μm ($PM_{2.5}$) had been significantly reduced nationwide (Wang et al., 2017). For example, the annual mean $PM_{2.5}$ concentration in Beijing dramatically reduced from 89.5 μg m^{-3} in 2013 to 42.0 μg m^{-3} in 2017 (Wang et al., 2020d; Zhang et al., 2019b). However, the average $PM_{2.5}$ concentration in China still far exceeds the guideline recommended by the World Health Organization (WHO, annual mean of 5.0 μg m^{-3}).

Reducing anthropogenic emissions can significantly decrease air pollution levels (Le et al., 2020; Wang et al., 2021a). For example, great improvements in air quality have been observed during the 2008 Olympics (Huang et al., 2010; Wang et al., 2010), the 2014 Asia-Pacific Economic Cooperation (APEC) meeting (Huang et al., 2015; Meng et al., 2015; Sun et al., 2016), the 2016 Hangzhou G20 summit (Li et al., 2018), and the 2015 China Victory Day Parade in Beijing (Ren et al., 2019; Zhao et al., 2017). The outbreak of the COVID-19 was followed by a strict nationwide lockdown in China, which has restricted anthropogenic activities such as transportation, commerce, and industry to prevent the spread of COVID-19 on a national scale. As a consequence, the emissions of primary air pollutants from anthropogenic sources were significantly reduced (Chen et al., 2020a; Le et al., 2020; Liu et al., 2020b; Lu et al., 2021; Ma et al., 2021). This was also observed as the spread of the COVID-19 pandemic worldwide (Baldasano, 2020; Kanniah et al., 2020; Lee et al., 2020; Otmani et al., 2020; Zhang et al., 2021a; Zoran et al., 2020). However, heavy air pollution events dominated by $PM_{2.5}$ still occurred during the COVID-19 lockdown in China (Huang et al., 2021; Li et al., 2021a; Liu et al., 2020b). This highlights the complexity and the nonlinearity between the primary and secondary pollutants in the atmosphere. The long-term lockdown period due to the COVID-19 pandemic provides us a good chance for understanding the chemistry connecting primary emissions to secondary pollutants formation.

The NCP region is one of the economic zones in China, while most affected by air pollution (Li et al., 2020; Sun et al., 2021b). Carbonaceous aerosol is one of the main components of atmospheric particulate matter, which is of great significance due to its role in climate change, earth's radiation balance, visibility, and human health (Bikkina et al., 2017; Li et al., 2009; Wang et al., 2020b; Wang et al., 2020e). Organic carbon (OC) is the main component (~90%) (Ram et al., 2008) of carbonaceous aerosols, while organic aerosol (OA) is an important contributor (20–90 wt%) to $PM_{2.5}$ (Cao et al., 2012; Sosa et al., 2017). OC can be directly emitted from various sources, such as traffic exhaust, biomass combustion, and plant respiration, and secondarily formed through photochemical or heterogeneous reactions in the atmosphere (Bae et al., 2004; Turpin and Huntzicker, 1995). Many previous works have discussed the concentration changes of air pollutants, such as O_3 (Kang et al., 2021; Lu et al., 2021), NO_2 and HONO (Liu et al., 2020b), $PM_{2.5}$ (Chen et al., 2020a; Zheng et al., 2020), heavy metal elements (Cui et al., 2020), light absorption components in $PM_{2.5}$ (Chen et al., 2020b), the source changes from biomass burning (Metya et al., 2020), and secondary formation (Huang et al., 2021; Sun et al., 2020b) during the lockdown period. However, there were few studies focusing on OC and the possible formation mechanism of SOC during the COVID-19 pandemic in the NCP region.

In this work, carbonaceous aerosols were semi-continuously measured in Beijing and Shijiazhuang, which are the typical cities in the NCP region, before and during the lockdown period of the COVID-19 pandemic. The effects of the lockdown on the concentrations, light absorption properties, formation mechanism, and potential sources of carbonaceous aerosols were discussed. This work will help for understanding the response of secondary formation of OC to emission reductions in the atmosphere.

2. Material and methods

2.1. Field measurements

Ground observations were conducted in Beijing and Shijiazhuang (Fig. S1) from December 1, 2019 to March 15, 2020, which covered the normal (December 1, 2019 to January 22, 2020) and the lockdown (January 23, 2020 to March 15, 2020) periods. The sampling site in Beijing is located at Aerosol and Haze Laboratory of Beijing University of Chemical Technology (AHL/BUCT, about 18 m from the ground, Lat. 39.97 and Lon. 116.42) (Cai et al., 2020; Chu et al., 2021; Liu et al., 2020c; Zhou et al., 2019) and the sampling site in Shijiazhuang is located at Hebei Atmospheric Super Station (HAS/SJZ, about 25 m from the ground, Lat. 38.03 and Lon. 114.61) (Liu et al., 2020b). Both cities are typical urban observation stations surrounded by traffic and residential emissions.

Mass concentration of $PM_{2.5}$ was measured by a beta attenuation mass monitor (BAM-1020, Met One Instruments) in Shijiazhuang and a Tapered Element Oscillating Microbalance (TEOM, ThermoFisher Scientific, 1405) in Beijing. Trace gases, including NO*x*, SO_2, CO, and O_3, were measured with corresponding analyzers (Thermo Scientific 42i, 43i, 48i, and 49i) in the two sites. Monitor for AeRosols and GAses in ambient air (MARGA, ADI 2080, Applikon Analytical B.V.) were used to measure water-soluble ions (Cl^-, NO_3^-, SO_4^{2-}, NH_4^+) in $PM_{2.5}$ in Shijiazhuang and a Time of-flight-Aerosol Chemical Speciation Monitor (ToF-ACSM) was used to measure non-refractory components (OA, Cl^-, NO_3^-, SO_4^{2-}, NH_4^+) in $PM_{2.5}$ in Beijing. Detailed information for ToF-ACSM has been described in previous works (Cai et al., 2020; Middlebrook et al., 2012).

Nitrate radical (NO_3) was measured with an iodide-based chemical ionization Atmospheric Pressure Interface Time-of-Flight Mass Spectrometer (CI-APi-TOF, Aerodyne Research, Inc.) at the AHL/BUCT station. The APi-TOF and CI-inlet has been well described in previous works (Jokinen et al., 2012; Junninen et al., 2010; Kurtén et al., 2011). Briefly, a 10 L min^{-1} of sample of air was drawn into the instrument through a 1/4 in. (O.D.) and 2 m (length) Teflon tubing, with the residence time of sample gas around 380 ms. 2 L min^{-1} of the sample gas was then drawn into the Ion-Molecule Reaction (IMR) unit. The main part of IMR was heated to 30 °C to reduce the wall loss of pollutants on the inner surface. In addition, the pressures in the IMR and Small Segmented Quadrupole (SSQ) were regulated to ~300 and ~2.5 mbar. This instrument can alternately measure gaseous species and particle-phase compounds after thermal desorption using a Filter Inlet for Gases and AEROsols (FIGAERO) (Lopez-Hilfiker et al., 2014). During the gas-phase sampling phase, it is able to detect the dinitrogen pentoxides (N_2O_5) in the cluster form of $(N_2O_5)I^-$ (Kercher et al., 2009). The concentration of NO_3 was calculated based on the equilibrium between NO_3 and N_2O_5 (Brown et al., 2006). The calibration of N_2O_5 was performed as same as that described in previous work (Wang et al., 2016), i.e., by injecting known concentration of N_2O_5 produced via mixing O_3 and NO_2.

OC and element carbon (EC) in $PM_{2.5}$ were measured at a 1-hour resolution using a semi-continuous thermo-optical transmittance (TOT)-based OC/EC analyzer (Model4, Sunset Laboratory Inc.). The principles and operating procedures have been described in detail elsewhere (Bae et al., 2004; Ji et al., 2018b; Klingshirn et al., 2019). An online parallel carbon stripper capable of removing volatile organic gases was installed upstream of the analyzer. Ambient air with a flow rate of 8 L min^{-1} was sampled through the $PM_{2.5}$ cyclone separator inlet and 3/8-inch steel tube into the OC/EC analyzer. $PM_{2.5}$ was collected hourly for 40 min on a baked round quartz fiber filter and then analyzed according to the NIOSH-5040 protocol (Birch and Cary, 1996). All carbons on the filter are thermally volatilized and oxidized to carbon dioxide (CO_2), then quantified sequentially using non-dispersive infrared (NDIR) detectors. The split point between OC and EC was determined by a 660 nm (Rattigan et al., 2010) laser to correct the artifacts in EC produced in the first stage. At the end of each sample, CO_2 was calibrated using methane equilibrated with 95% helium. Additional calibrations were performed monthly with known amounts of sucrose and weekly with zero calibration. Black carbon (BC) was measured

with a seven-band Aethalometer (AE33, Magee Scientific) in both sites. The AE33 has been widely used to continuously measure aerosol light absorption at 370, 470, 520, 590, 660, 880, and 950 nm (Helin et al., 2021; Jing et al., 2019; Lin et al., 2021). The principle and more details of AE33 can be found in previous work (Drinovec et al., 2015).

Meteorological parameters including temperature (T), pressure, relative humidity (RH), wind speed (WS), and wind direction (WD) were measured using a meteorological station (WXT520, Visala) in Shijiazhuang and an automatic weather station (QML201C and PWD22 Vaisala) in Beijing. Mixing boundary layer height (MLH) was measured using a Doppler Lidar (EV-Lidar-CAM, Everise Technology Ltd.) in Shijiazhuang and ceilometer (CL51, Vaisala) in Beijing.

2.2. Data treatment and analysis

2.2.1. SOC estimation by minimum R squared (MRS) method

POC is usually emitted from primary emission sources, including vehicular emissions, biomass burning, and cooking emissions. SOC can be formed through the oxidation of POC and volatile organic compounds (VOCs). The EC tracer method (Turpin and Huntzicker, 1995; Zhao et al., 2013) has been widely used to estimate the mass concentration of SOC using the following equation, in which combustion is assumed to be the only source of EC.

$$\mathrm{POC} = (\mathrm{OC/EC})_{pri} \times \mathrm{EC} \quad (1)$$

$$\mathrm{SOC} = \mathrm{OC}_{total} - \mathrm{POC} \quad (2)$$

Thus, the first step is to find the appropriate ratio of primary OC/EC, i.e., $(\mathrm{OC/EC})_{\mathrm{pri}}$ (Turpin and Huntzicker, 1995). In most of these previous studies, the lowest value (5–20%) of OC/EC was used empirically (Yao et al., 2020; Zhang et al., 2019a). In this study, the appropriate value of $(\mathrm{OC/EC})_{\mathrm{pri}}$ was determined using the MRS method (Bian et al., 2018; Ji et al., 2018b; Millet et al., 2005; Sun et al., 2020a; Wu and Yu, 2016), which determining the $(\mathrm{OC/EC})_{\mathrm{pri}}$ when the smallest correlation coefficient (R^2) between SOC and EC achieved by assuming a series of continuous OC/EC ratios. More details can be found elsewhere (Wu et al., 2019; Wu and Yu, 2016; Yao et al., 2020). The actual $(\mathrm{OC/EC})_{\mathrm{pri}}$ corresponding to the minimum R^2 (SOC vs. EC) are shown in Fig. S2. The monthly $(\mathrm{OC/EC})_{\mathrm{pri}}$ values in Shijiazhuang were 3.14, 2.43, 4.91, and 3.28, respectively, in December 2019, January 2020, February 2020, and March 2020. The corresponding values in Beijing were 2.70, 2.88, and 2.96 for December 2019, January 2020, and February 2020, respectively. The $(\mathrm{OC/EC})_{\mathrm{pri}}$ value in March 2020 was absent due to the miss of OC data.

In addition, positive matrix factorization (PMF) was applied to confirm the SOC results in Beijing. An IgorPro program (Wavemetrics, ver. 6.3.7.2) based the Source Finder toolkit (SoFi, ver. 6.8.4) with a multi-linear engine (ME-2) was used to execute the PMF analysis and evaluate the results. Detailed information of SoFi and PMF calculations are described elsewhere (Cai et al., 2020; Canonaco et al., 2013; Daellenbach et al., 2016).

2.2.2. The light absorption data

BC was measured using an aethalometer (AE33, Magee Scientific), which has seven bands at 370, 470, 520, 590, 660, 880, and 950 nm. Brown carbon (BrC) was calculated according to the previous works (Virkkula et al., 2015; Zhang et al., 2021b). Briefly, the mass absorption cross-section (MAC) values were 18.47, 14.54, 13.14, 11.58, 10.35, 7.77, and 7.19 $\mathrm{m^2 g^{-1}}$ for the corresponding wavelengths in AE33. The absorption coefficient (b_{abs}) at different λ was calculated according to Eq. (3):

$$b_{abs,\lambda} = \mathrm{BC}_{output,\lambda} \times \mathrm{MAC}_{BC,\lambda} \quad (3)$$

where, $\mathrm{BC}_{output,\lambda}$ is the mass concentration of BC at wavelength λ nm. Absorption Ångström exponent (AAE) has been widely used to describe the wavelength dependence of light absorb aerosol (Lack and Langridge, 2013; Laskin et al., 2015; Liu et al., 2018; Wang et al., 2020c). It can be calculated according to Eq. (4):

$$b_{abs} = \mathrm{K} \times \lambda^{-AAE} \quad (4)$$

where, K is a constant value. It should be noted that non-BrC coating on BC could also lead to increased AAE (Garg et al., 2016; Lack and Langridge, 2013). However, lots of researches usually suggested that the AAE value of BC is about 1 (Lack and Langridge, 2013; Liu et al., 2018). At long wavelengths, such as 880 and 950 nm, BrC does not absorb light (Kirchstetter et al., 2004; Liakakou et al., 2020). Thus, the absorption of BC and BrC can be calculated according to Eqs. (5) and (6), respectively:

$$b_{abs,BC,\lambda} = b_{abs,BC,880} \times \left({}^{880}/_{\lambda}\right)^{AAE_{BC}} \quad (5)$$

$$b_{abs,BrC,\lambda} = b_{abs,\lambda} - b_{abs,BC,\lambda} \quad (6)$$

2.2.3. Backward trajectory and PSCF model analysis

To understand the potential source regions, we performed a 48-hour backward trajectory analysis using the National Oceanic and Atmospheric Administration (NOAA) Hybrid Single-Particle Lagrangian Integrated Trajectory (HYSPLIT) model. The time interval was set to 1 h. The National Centers for Environmental Prediction (NCEP) Global Data Assimilation System (GDAS) data (ftp://arlftp.arlhq.noaa.gov/pub/archives/) with a spatial resolution of 1° × 1° were input to the HYSPLIT model. 100 m (Dimitriou and Kassomenos, 2016) was used as the arriving height. 2544 trajectories were obtained. The Potential Source Contribution Function (PSCF) analysis was carried out based on the above generated backward trajectories using the TrajStat software (http://meteothink.org/index.html) (Wang, 2014, 2019; Wang et al., 2009) to identify the source strength of a geographical area. Weighting functions were used to minimize the uncertainty of PSCF analysis and referred to as WPSCF (Polissar, 1999; Sun et al., 2019a).

3. Results and discussion

3.1. Overview of the air quality during observation

Fig. 1 shows the time series of various pollutants and meteorological parameters in Beijing and Shijiazhuang, including NO, NO_2, O_3, T, RH, WS, WD, and MLH. Because of the lack of OA data in the Shijiazhuang site, the OA was replaced with organic matter (OM, 1.5 × OC) (Countess et al., 1980; Japar et al., 1984; Ren et al., 2021; Xing et al., 2013). During the lockdown period, the mean $PM_{2.5}$ concentrations in Shijiazhuang decreased by 15.2% (from 114.3 ± 84.6 to 97.0 ± 75.1 μg $\mathrm{m^{-3}}$) with respect to the normal period. By contrast, the mean $PM_{2.5}$ concentrations in Beijing increased considerably (52.4%, from 41.9 ± 39.7 to 63.9 ± 58.3 μg $\mathrm{m^{-3}}$) during the lockdown period compared with that in the normal period (Fig. 1A and E). The mean concentrations of NO and NO_2 decreased sharply compared to these in the normal period in both Shijiazhuang (87.9 and 41.8%, from 22.2 and 26.5 ppb to 2.7 and 15.5 ppb) and Beijing (82.2 and 59.6%, from 20.1 and 31.0 to 3.6 and 12.5 ppb). This is in agreement with the strict controls on anthropogenic emissions during the lockdown period. However, O_3 concentrations increased 176.0% (from 11.7 to 32.2 ppb) in Shijiazhuang and 241.2% (from 7.4 to 25.1 ppb) in Beijing (Fig. 1B and F).

Long-term stagnant meteorological conditions, including high RH, low WS, and low MLH, result in the accumulation of pollutants, subsequently, lead to the high occurrence of haze pollution during the lockdown periods (Chen et al., 2020b; Le et al., 2020; Liu et al., 2020b; Sun et al., 2019b). As shown in Fig. S3, the wind speeds in Beijing are significantly lower than that in Shijiazhuang, which means the air mass in Beijing will be more readily affected by the adverse meteorological conditions than that in Shijiazhuang. This could be the reason why the mean concentration of $PM_{2.5}$ increased at the beginning of the lockdown period compared to the

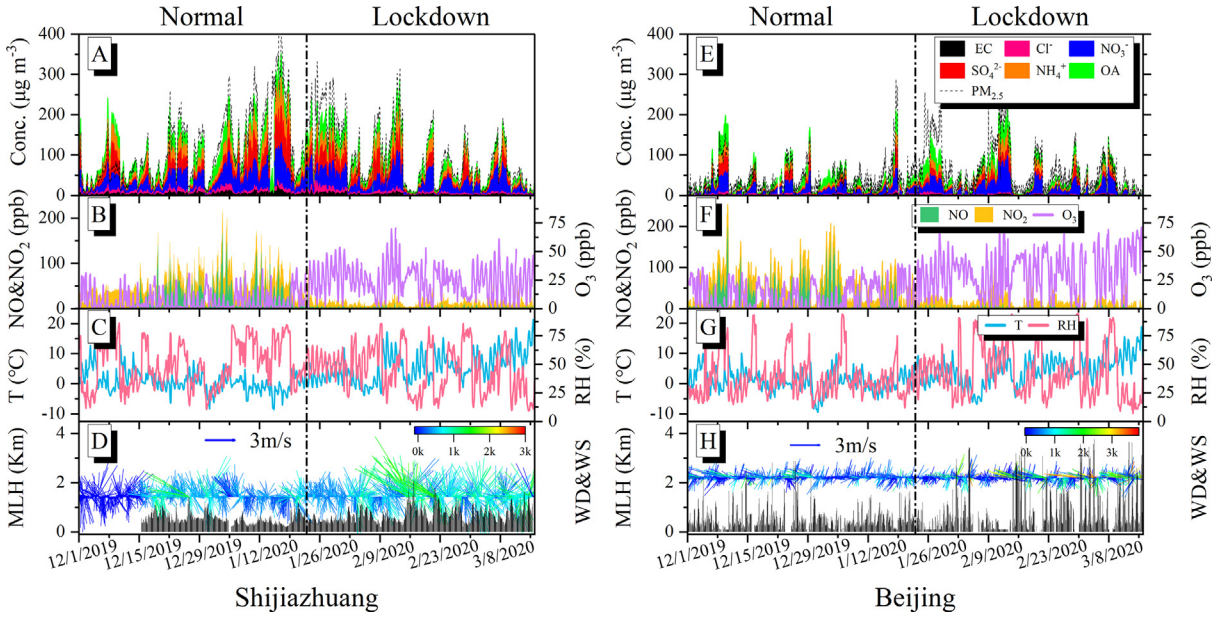

Fig. 1. Time series of components of $PM_{2.5}$, NO, NO*x*, O_3, T, RH, WD, WS, and MLH in Shijiazhuang (A–D) and Beijing (E–H), the wind data was colored by MLH. The dash line divided the normal and the lockdown period.

normal period in Beijing, while a reduction was observed in Shijiazhuang. In addition, the relative contributions of local pollution and regional transport are varied. For the first pollution episode in Beijing, it is mainly due to the aggravation of local pollution, while the contribution of regional transport increased considerably in the second pollution episode (Zhao et al., 2020). It should be noted that the mean of MLH increased 29.3% (from 555.8 ± 233.3 to 718.9 ± 315.2 m) in Shijiazhuang and 55.4% (from 529.4 ± 419.1 to 822.4 ± 867.3 m) in Beijing during the lockdown period. In addition, the mean wind speed increased 30.8% (from 1.35 ± 0.73 to 1.77 ± 0.97 m s^{-1}) in Shijiazhuang and 10.6% (from 0.75 ± 0.55 to 0.82 ± 0.57 m s^{-1}) in Beijing. Thus, considering the improvement of dispersion ability, the concentrations of secondary pollutants ($PM_{2.5}$ and O_3) should decrease in both Shijiazhuang and Beijing during the lockdown period. The chemistry process should thus play important roles in both the elevated $PM_{2.5}$ and O_3 during the lockdown period.

NO*x* is the precursors of nitrate, which is the dominator of $PM_{2.5}$ mass in the NCP region (Li et al., 2021b; Tao et al., 2017). This means that a decrease in NO*x* concentration might be beneficial to $PM_{2.5}$ reduction. However, two large-scale $PM_{2.5}$ pollution episodes (Zhao et al., 2020) still occurred in the NCP region (Fig. 1A and E) at the beginning of the lockdown period although NO*x* showed a significant reduction in the COVID-19 episode. This is consistent with previous results that emergency measures for severe haze prevention can only weakly reduce $PM_{2.5}$ concentration (Ma et al., 2020; Wang et al., 2020a). Previous works also suggested that the chemical transformation of gaseous pollutants to secondary inorganic aerosols may lead to the explosive growth of $PM_{2.5}$ (Chen et al., 2020a; Sun et al., 2019b; Wang et al., 2013; Zheng et al., 2015; Zhong et al., 2018). As shown in Fig. S4B, nitrate was the dominant contributor to inorganic salts during the whole campaign. This is consistent with previous observations during the COVID-19 lockdown in north China (Huang et al., 2021). The nitrogen oxidation ratio (NOR), which is calculated from the molar ratios of the particulate concentration and the sum of gaseous and particulate concentrations,

$$NOR = m(NO_3)/[m(NO_3) + m(NO_x)] \quad (7)$$

showed a significant increase of 109.6% (from 0.2 ± 0.2 to 0.5 ± 0.2) in Shijiazhuang and 40.2% (from 0.5 ± 0.2 to 0.7 ± 0.2) in Beijing (Fig. S5). This indicates the increase of atmospheric oxidation capacity during the lockdown period in both Shijiazhuang and Beijing. Chen et al. (2020a) reported that the diurnal variation of NOR in Shanghai showed a prominent peak at midnight, which indicates the importance of nocturnal reactions to nitrate production.

NO*x* is also one of the precursors of O_3. Huang et al. (2021) pointed out that the significant reduction of NO*x* emissions from transportation led to the generation of O_3 and nocturnal NO_3 radicals during the lockdown period (Huang et al., 2021; Zhao et al., 2020). The increase in O_3 concentration (Fig. 1B and F), which is from the nonlinear photochemical reactions between NO*x* and VOCs (Le et al., 2020; Nichol et al., 2020), also suggests an enhanced oxidation capacity. O*x* (O_3 + NO_2) has been widely used to estimate the total atmospheric oxidation capacity (Chen et al., 2020a; Kley et al., 1994; Leighton, 2012; Notario et al., 2013). Meanwhile, carbon monoxide (CO) has a long lifetime against oxidation by OH radicals and thus can be used as a reasonable tracer of primary emissions to account for atmospheric dilution (De Gouw and Jimenez, 2009; DeCarlo et al., 2010). Thus, the ratios of other pollutant species to CO can partially eliminate the boundary layer effect (Yao et al., 2020). Fig. S4A shows the CO normalized atmospheric oxidant capacity (O*x*/CO) during the whole campaign. Compared with the normal period, the atmospheric oxidation capacity during the lockdown period increased significantly in both sites. In addition, as shown in Fig. S4B, OA is always the most important contributor to $PM_{2.5}$ in both Shijiazhuang and Beijing. For example, the fraction of OA in $PM_{2.5}$ was 28.9% in Shijiazhuang and 34.6% in Beijing, respectively, during the lockdown period. In previous work, attention was mainly paid to the formation of secondary inorganic aerosol during the COVID-19 lockdown (Chen et al., 2020a; Lu et al., 2021), while less attention was paid to organic aerosol formation. In the following sections, we will focus on the evolution of OA component.

3.2. Increase of nocturnal SOC during lockdown periods

The mean concentration of OA showed a decrease of 17.6% (from 23.3 ± 12.9 to 19.2 ± 13.4 μg m^{-3}) in Shijiazhuang, while a slight increase of 7.6% (from 13.4 ± 12.2 to 14.4 ± 12.9 μg m^{-3}) in Beijing during the lockdown period. Interestingly, OA showed a less decreased amplitude in Shijiazhuang or a more increase amplitude in Beijing in the nighttime compared with the daytime (Fig. S6). This implies that there should have an additional OA source in the NCP region.

Fig. S7 shows the mean concentrations of OC, EC, POC, and SOC during different periods. The mean concentrations of OC, EC, and POC of

Shijiazhuang were 12.9 ± 8.9, 3.6 ± 2.3, and 7.7 ± 5.3 μg m^{-3}, respectively, during the lockdown period, which was 17.8, 32.7, and 30.6% lower than those during the normal period (15.7 ± 8.5, 5.3 ± 3.1, and 11.1 ± 6.1 μg m^{-3}). However, the SOC concentration increased by 13.6% (from 4.6 ± 4.3 to 5.2 ± 6.3 μg m^{-3}) in Shijiazhuang. In Beijing, the concentrations of OC, EC, and SOC increased significantly ($P < 0.05$) during the lockdown period. As mentioned above (Fig. 1), Beijing was more readily affected by the adverse meteorological conditions and regional transport of airmass than Shijiazhuang. The increase of the concentrations of OC and EC in Beijing might be related to the transport of the regional background although the anthropogenic emissions were reduced. The mean concentrations of SOC in both two sites showed significant increases contrasting with the reduction of POC during the lockdown period. This means that the secondary formation of OC was enhanced during the lockdown period while anthropogenic activities were suppressed.

Fig. 2 shows the diurnal patterns of OC, EC, POC, SOC, and SOC/OC during the normal (black dots and lines) and the lockdown periods (the red dots and lines). The area between the diurnal pattern lines means the difference of the pollutant between the lockdown period and the normal period. The yellow color indicates a positive difference, while the blue one means a negative difference. Both OC and EC showed a bimodal diurnal distribution. The peaks appeared at 09:00 and 02:00, respectively, in Shijiazhuang, while they occurred at 10:00 and 21:00 in Beijing. POC and EC are solely from primary emissions (De Gouw and Jimenez, 2009; Safai et al., 2014). In Shijiazhuang, the diurnal patterns of POC and EC changed little during the two periods. Thus, their differences remained stable (Fig. 2B and C). These results indicate that the emission intensity of EC and POC were reduced, while their emission patterns should remain during the lockdown period when compared with that during the normal period. However, OC and SOC showed different diurnal patterns during the normal and the lockdown period (Fig. 2A and D), especially in the nighttime. Either a larger yellow difference of SOC (Fig. 2D) or a lesser blue difference of OC (Fig. 2A) in nighttime indicates a strong nocturnal SOC source during the lockdown period. The diurnal patterns of SOC in Beijing (Fig. 2I) were similar to those in Shijiazhuang. In addition, the nighttime increase of the SOC during the lockdown period related to the normal period in Beijing (65.4%, from 1.3 ± 1.1 to 2.1 ± 2.6 μg m^{-3}) was even more remarkable when compared with that in Shijiazhuang (23.2%, from 4.6 ± 4.4 to 5.7 ± 6.6 μg m^{-3}). Moreover, the SOC/OC in Beijing (Fig. 2J) showed a similar diurnal variation as SOC, i.e. a distinct nocturnal increase, especially in Beijing. The diurnal variation of SOC/OC showed a remarkable increase in both daytime and nighttime in Shijiazhuang (Fig. 2E), which resulting into a weak difference between the daytime and nighttime SOC/OC ratios. This obvious enhancement of the nocturnal SOC/OC might be related to the primary emissions, subsequently, strong photochemical formation of SOA during the normal period in Beijing (Kuang et al., 2020). Therefore, we speculate that the increase of nighttime SOC concentration should be related to nocturnal chemistry.

To verify the speculation mentioned above, PMF of OA measured using an ACSM in Beijing was performed. Four factors including more-oxidized aerosol (MOOA), less-oxidized organic aerosol (LOOA), cooking organic aerosol (COA), and fossil fuel aerosol (FFOA) were obtained. The time series and diurnal variations of the four factors are presented in Fig. S8 and S9. SOA (MOOA + LOOA) was significantly higher during the lockdown period than that in the normal period (Fig. S9), which is consistent with the change of SOC (Fig. 2H). Meanwhile, the diurnal pattern of SOA showed a more significant increase in the night like that of SOC (Fig. 2H) during the lockdown period when compared to the normal period. Furthermore, the diurnal variation of primary organic carbon (POA, FFOA + COA) derived from ACSM-PMF showed a reduction during the lockdown period. In addition, the SOA also showed a good correlation (R^2 = 0.55, Fig. S10) with SOC in polluted episodes (with $PM_{2.5}$ higher than 75 μg m^{-3}) during the whole campaign. These results reveal that the conclusions based on SOC analysis are reasonable. In addition, it suggests the nocturnal chemistry is important in OA formation during the lockdown period.

3.3. Nocturnal atmospheric oxidation changes during COVID-19 pandemic

NO_3 radicals were the essential nocturnal oxidants in the atmosphere (Brown et al., 2003). In Beijing, the NO_3 radical concentrations were measured using a CI-APi-TOF. The measured NO_3 radicals in Beijing showed a

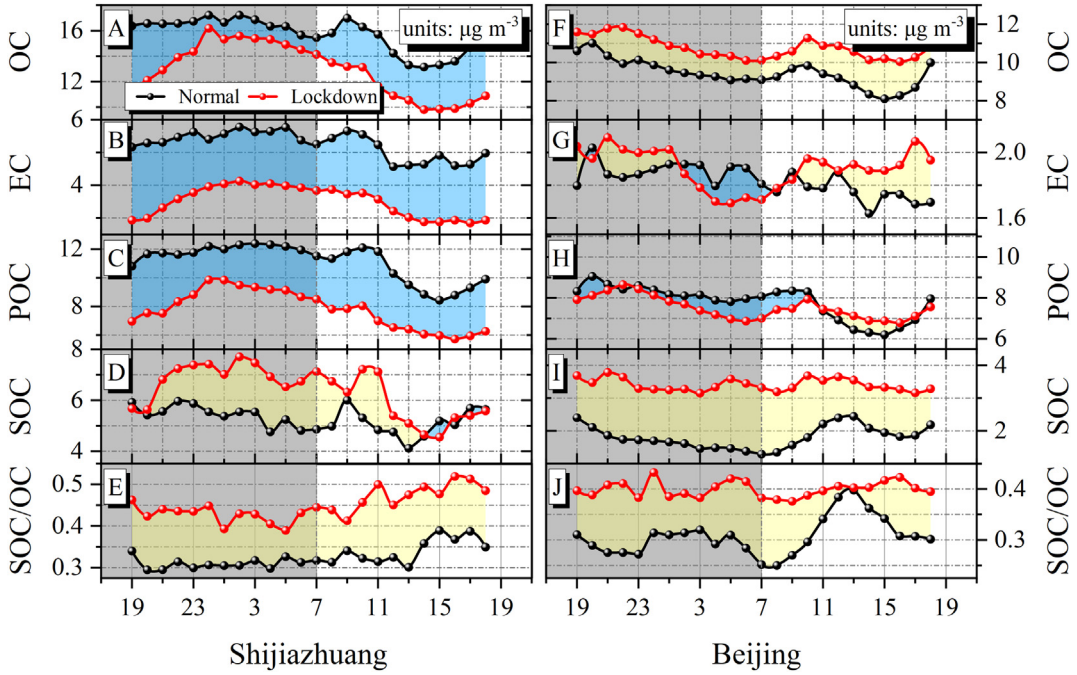

Fig. 2. The mean diurnal cycle of carbonaceous aerosol components: OC, EC, POC, SOC, and SOC/OC in Shijiazhuang (A–E) and Beijing (F–J) during the normal period (black line) and the lockdown period (red line). The unit of the species is μg m^{-3}. The shadow area indicates nighttime. The area between the two lines is filled with blue or yellow to distinguish the relative change of the difference between the normal period and the lockdown period. The yellow color indicates a positive difference, while the blue one means a negative difference.

significant increase from 0.6 ± 1.2 ppt in the normal period to 2.5 ± 5.1 ppt in the lockdown period (Fig. 3A). Meanwhile, the nocturnal NO_3 concentration was ~3 times higher than that in the daytime (Fig. 3B). This means the nighttime oxidation capacity also increased during the lockdown period in Beijing.

Unfortunately, NO_3 radical measurements were unavailable in the Shijiazhuang. As for the sources of NO_3 radicals in the atmosphere, there is an equilibrium between NO_3 and N_2O_5, while N_2O_5 is formed from the reaction between NO_2 and O_3. On the other hand, the reaction between NO and NO_3 is an important sink of NO_3 radicals. Thus, we use $O_3 \times NO_2$/NO as a proxy of NO_3 concentration in the atmosphere (Brown et al., 2003). As shown in Fig. 3, although the absolute values are different between the measured NO_3 concentrations and the proxy of NO_3 radicals in Beijing, the estimated NO_3 radicals show a similar variation trend during different periods. At the same time, the diurnal patterns of the estimated NO_3 are also similar to that of the measured NO_3 (Fig. 3). Thus, we further estimated the NO_3 concentrations in Shijiazhuang (Fig. S11). It showed similar diurnal curves like Beijing. Obviously, the nocturnal NO_3 concentrations in both Beijing and Shijiazhuang significantly increased during the lockdown period when compared with the normal period. This can be explained by the reduction of NO and the increase of O_3 on a regional scale (Kang et al., 2021). In addition, the mean concentration of SOA increased as a function of NO_3 radical concentration when SOA concentrations were higher than 20 μg m^{-3}, usually occurred in the lockdown period (Fig. S12). This phenomenon clearly illustrates that the atmospheric oxidation capacity was significantly increased in the lockdown period compared to the normal period. Therefore, we can ascribe the enhanced SOC formation in the lockdown period than the normal period to nocturnal chemistry related to NO_3 radicals although more evidence such as SOA tracers associated with nocturnal NO_3 radicals are required in the future.

3.4. Impact of COVID-19 on aerosol light absorption

Aerosol light absorption significantly influences on the earth's climate, tropospheric chemistry, and visibility (Ding et al., 2016; Sun et al., 2021a; Watson, 2002). BC and BrC, which play essential roles in the global radiative balance of the earth's atmosphere (Andreae and Gelencser, 2006; Bond, 2001), are the two fundamental optical carbon matters in $PM_{2.5}$. BC has been considered the most effective climatic forcing agent, with broadband absorption properties (Bond et al., 2013). BrC, as a kind of light-absorbing OC, shows a wavelength-dependent absorption that peaks in the ultraviolet (UV) spectral region and declines sharply in the visible spectral region (Andreae and Gelencser, 2006; Laskin et al., 2015). Both BC and BrC can be emitted directly from the combustion of fossil fuels and biomass burning, while BrC can also be formed in atmospheric chemical processes (e.g., multi-phase reactions between gas-phase, particles, and in-cloud processes) (Andreae and Gelencser, 2006; Harrison et al., 2005; Laskin et al., 2015; Wang et al., 2019; Zhang et al., 2013b). The absorption of BrC at 370 nm ($b_{abs,\ BrC}$(370 nm)) was the most intensive in the seven wavelengths and regarded as the representative value of BrC absorption (Lin et al., 2021; Wang et al., 2019). In addition, the light absorption at 880 nm ($b_{abs,\ BC}$(880 nm)) was the most representative value of BC absorption due to BrC doesn't absorb at 880 nm (Drinovec et al., 2015; Lin et al., 2021). Hence, the light absorption at 370 and 880 nm was used to explore the optical properties of BrC and BC.

Fig. S13 shows the light absorption at the different wavelengths of BC and BrC during the normal and the lockdown periods. The mean b_{abs} (880 nm) decreased from 31.2 ± 18.1 to17.3 ± 11.8 Mm^{-1} (44.6%) and 21.0 ± 19.3 to 19.0 ± 16.1 Mm^{-1} (9.6%) in Shijiazhuang and Beijing, respectively, during the lockdown period. This illustrates the significant reduction of anthropogenic emissions during the lockdown period, especially from traffic exhaust. At the same time, the light absorption at 370 nm ($b_{abs,\ total}$(370 nm)) decreased by 42.4% (from 115.4 ± 64.9 to 66.5 ± 50.4 Mm^{-1}) in Shijiazhuang during the lockdown period compared with that in the normal period because BC was the dominator of the light absorption substances even at 370 nm (Fig. S13). As shown in Fig. 2, although SOC increased significantly during the lockdown period in Shijiazhuang, both POC and EC significantly decreased. Thus, the significant decrease of light absorption in Shijiazhuang should be contributed to the decreases of POC and BC or EC due to anthropogenic emissions reductions. However, the $b_{abs,\ total}$(370 nm) in Beijing showed a slight increase (3.9%, from 76.1 ± 63.4 to 79.2 ± 67.3 Mm^{-1}) during the lockdown period. This can be explained by a slight decrease in POC and an obvious increase in SOC in Beijing (Fig. 2). The relative contribution of BrC to total absorption at 370 nm showed a slight increase of 2.5% (from 35.8% to 38.2%) in Shijiazhuang and 3.8% (from 36.8% to 40.6%) in Beijing, respectively, during the lockdown period (Fig. S13). This implies that secondary formation during regional transport of airmass might also contribute to the light adsorption of organic matters.

Fig. 4 shows the diurnal variations of the light absorption of BrC measured at 370 nm ($b_{abs,\ BrC}$(370 nm)). In Shijiazhuang, the $b_{abs,\ BrC}$ (370 nm) showed a similar diurnal pattern during the lockdown period like that during the normal period, while the absolute values during the lockdown period decreased significantly (Fig. 4A). The nighttime decrease of the $b_{abs,\ BrC}$(370 nm) between these two periods was slightly smaller than the daytime counterpart in Shijiazhuang. In Beijing, besides a slight increase of the $b_{abs,\ BrC}$(370 nm) during the lockdown period, the nighttime increase of the $b_{abs,\ BrC}$(370 nm) between these two periods was obviously higher than that in the day (Fig. 4B). Fig. S14 shows the fraction of BrC in the total light adsorption at 370 nm. The diurnal pattern of the fraction of $b_{abs,\ BrC}$(370 nm) showed a larger increase rate in nighttime during the lockdown period compared with that during the normal period in Shijiazhuang

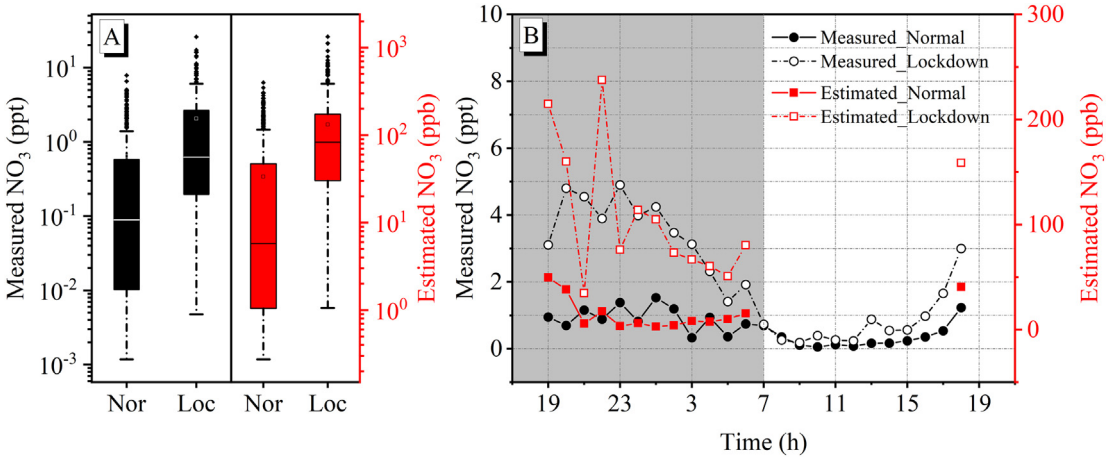

Fig. 3. (A) The concentration and (B) diurnal variations of measured and estimated NO_3 radicals of Beijing site.

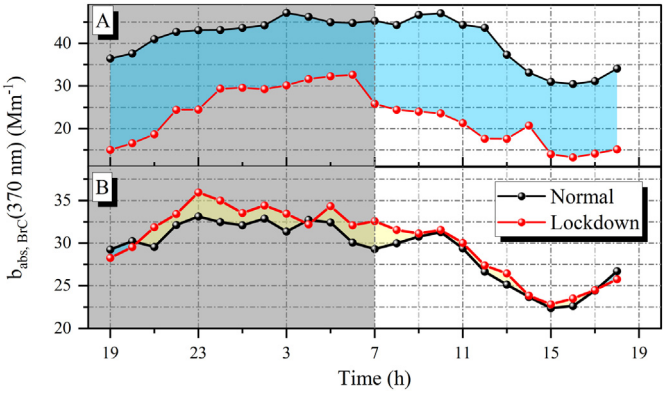

Fig. 4. The $b_{abs,\ BrC}$(370 nm) diurnal variation of BrC of during the normal period (black line) and the lockdown period (red line) in (A) Shijiazhuang and (B) Beijing. The shadow area is used to indicate nighttime. The area between the two lines is filled with blue or yellow to distinguish the relative size of the different value between the normal period and the lockdown period. The yellow color indicates a positive difference, while the blue one means a negative difference.

(Fig. S14A). A similar phenomenon was observed at the Beijing site (Fig. S14B). These results imply that the nocturnal oxidation of VOCs or POC by NO_3 radicals might contribute to BrC generation. In addition, $b_{abs,\ BrC}$(370 nm) showed a good correlation with SOC in polluted episodes ($PM_{2.5} > 75\ \mu g\ m^{-3}$) during the lockdown period ($R^2 = 0.51$, Fig. S15), which was similar to the scatter plot of SOA vs. SOC (Fig. S10). Thus, it is reasonable to propose that BrC was an important contributor to SOC.

3.5. Backward trajectory and PSCF analysis of SOC

The potential sources are further analyzed for understanding the difference of SOC between the normal and the lockdown periods in the NCP region. The domain is from 70° E to 125° E and 30° N to 60° N, which was divided into 26,400 grid cells of 0.25° × 0.25° latitude and longitude. The PSCF analysis for the hourly SOC data can provide information on regional transport and local emissions for carbonaceous aerosols. Fig. S16 shows the PSCF results of Shijiazhuang and Beijing during different periods. For Shijiazhuang, the areas with a high weighted potential source of SOC (with contribution function values >0.8) included Shijiazhuang and the regions between Hebei and Shanxi provinces (Fig. S16A and B), which agreed well with previous studies (Wang et al., 2018; Xie et al., 2019; Zong et al., 2018). For Beijing (Fig. S16C and D), the main potential source areas of SOC were Beijing, the center of Inner Mongolia, the northern Shanxi province, and the central region of the Hebei province (Ji et al., 2018a; Zhang et al., 2013a). It has been pointed out that those potential areas were heavily polluted areas due to intensive pollutant emissions from industry, resident coal combustion and vehicle exhaust (Bie et al., 2021; Ji et al., 2018a; Xie et al., 2019; Zong et al., 2018).

To understand the variations of potential sources of SOC during lockdown periods, we subtracted the PSCF result during the normal period from that during the lockdown period (Fig. 5). Regions with a difference between 0.1 and −0.1 are denoted as colorless, which means that these regions contribute almost the same during normal and lockdown periods. The red color represents positive values, while the blue one represents negative. Lager absolute values represent a more significant difference of contribution in SOC. For Shijiazhuang, the southern areas of Shanxi province and the central regions of Inner Mongolia contribute more to the potential source of SOC in the normal period than that in the lockdown period, while Tianjin, Beijing, the eastern of Hebei province, the northern of Shandong province, and the southern of Liaoning province contribute more to SOC during the lockdown period. For Beijing, the contribution of central and western of Inner Mongolia (extend to the Mongolian regions) were decreased, while Tianjin, the southern of Hebei, the northern of Shanxi province, the northern of Shandong province, and the southern of Liaoning province contribute more during the lockdown period. Overall, the southeast regions of the NCP (including Beijing and Shijiazhuang) were the dominate contributors to SOC during the lockdown period, while a slight difference between these two locations was observable due to the different prevailing wind directions and the surrounded industry distribution.

4. Conclusion

The anthropogenic emissions in the NCP region were greatly reduced during the lockdown period caused by the COVID-19 pandemic, such as POC, NO, and NO_2 in Shijiazhuang (30.6, 87.9, and 41.8%) and in Beijing (4.0, 82.2, and 59.6%). However, the particle matter showed an unexpected increase during the lockdown period due to the adverse meteorological conditions and regional transport of airmass in Beijing. An increase in atmospheric oxidation capacity was observed during the lockdown period. The increased O_3 concentrations in Shijiazhuang (176.0%) and in Beijing (241.2%) were mainly due to the nonlinear O_3 production chemistry and the reduced titration of ozone by NO.

SOC significantly increased during the lockdown period in both Shijiazhuang (13.6%) and Beijing (53.0%) although the anthropogenic emissions drastically reduced. The diurnal pattern of SOC, SOA, and the absorption of BrC suggested an additional nighttime SOC source during the lockdown period in the NCP region. NO_3 radicals should play an important role in the formation of SOC in the nighttime because the nocturnal NO_3

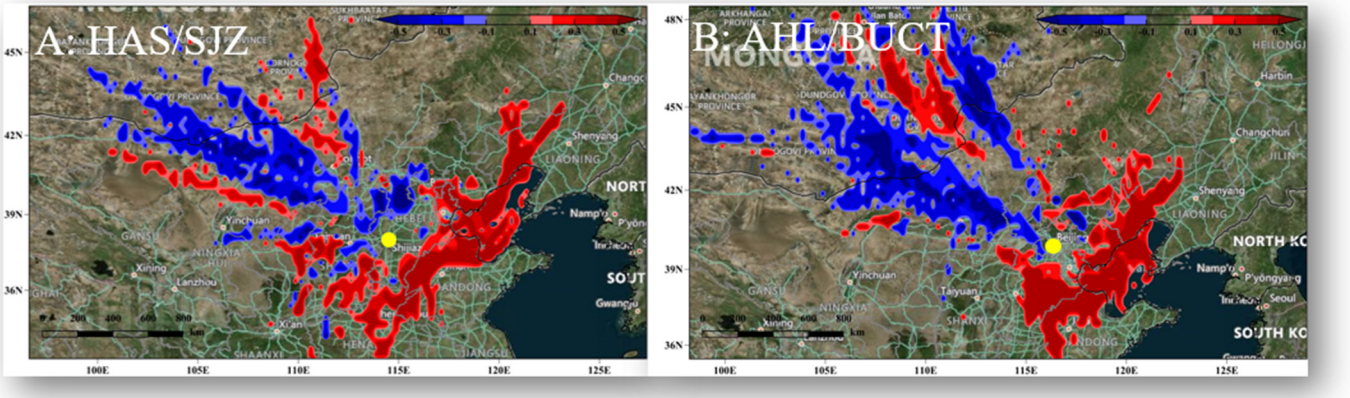

Fig. 5. Weighted potential source contribution function (WPSCF) difference value map for SOC arriving in the (A) Shijiazhuang and (B) Beijing region at the height of 100 m between the lockdown and normal periods.

concentrations increased significantly during the lockdown period when compared with that in the normal period. The southeast regions of NCP, northern regions of Shandong province, and the southern regions of Liaoning contributed more to the SOC during the lockdown period than the normal period. Our results mean that more attention should be paid to the nocturnal chemistry for further reduction PM concentration in China.

CRediT authorship contribution statement

Zemin Feng: Writing - original draft, Conducting experiments, Data curation. **Feixue Zheng**: Investigation, Data curation. **Yongchun Liu**: Conceptualization, Methodology, Data curation, Writing - review & editing. **Xiaolong Fan**: Investigation, Data curation. **Chao Yan**: Investigation, Data curation. **Yusheng Zhang**: Investigation, Data curation. **Kaspar R. Daellenbach**: Investigation, Data curation. **Federico Bianchi**: Investigation, Data curation. **Tuukka Petäjä**: Investigation, Data curation. **Markku Kulmala**: Investigation, Data curation. **Xiaolei Bao**: Investigation, Methodology, Data curation. All authors contributed to the paper with useful scientific discussions or comments.

Declaration of competing interest

The authors declare that they have no known competing financial interests or personal relationships that could have appeared to influence the work reported in this paper.

Acknowledgments

This research was financially supported by the National Natural Science Foundation of China (41877306, 92044301), the Ministry of Science and Technology of the People's Republic of China (2019YFC0214701), Academy of Finland via Center of Excellence in Atmospheric Sciences (272041, 316114, and 315203) and European Research Council via ATM-GTP 266 (742206), the Hebei Technological Innovation Center for Volatile Organic Compounds Detection and Treatment in Chemical Industry (ZXJJ20210403), the Strategic Priority Research Program of Chinese Academy of Sciences and Beijing University of Chemical Technology.

Appendix A. Supplementary data

Supplementary data to this article can be found online at https://doi.org/10.1016/j.scitotenv.2021.152191.

References

Andreae, M.O., Gelencser, A., 2006. Black carbon or brown carbon? The nature of light-absorbing carbonaceous aerosols. Atmos. Chem. Phys. 6, 3131–3148. https://doi.org/10.5194/acp-6-3131-2006.

Bae, M.S., Schauer, J.J., DeMinter, J.T., Turner, J.R., Smith, D., Cary, R.A., 2004. Validation of a semi-continuous instrument for elemental carbon and organic carbon using a thermal-optical method. Atmos. Environ. 38, 2885–2893. https://doi.org/10.1016/j.atmosenv.2004.02.027.

Baldasano, J.M., 2020. COVID-19 lockdown effects on air quality by NO2 in the cities of Barcelona and Madrid (Spain). Sci. Total Environ. 741, 140353. https://doi.org/10.1016/j.scitotenv.2020.140353.

Bian, Q., Alharbi, B., Shareef, M.M., Husain, T., Pasha, M.J., Atwood, S.A., Kreidenweis, S.M., 2018. Sources of PM2.5 carbonaceous aerosol in Riyadh,Saudi Arabia. Atmos. Chem. Phys. 18, 3969–3985. https://doi.org/10.5194/acp-18-3969-2018.

Bie, S., Yang, L., Zhang, Y., Huang, Q., Li, J., Zhao, T., Zhang, X., Wang, P., Wang, W., 2021. Source appointment of PM2.5 in Qingdao Port, East of China. Sci. Total Environ. 755, 142456. https://doi.org/10.1016/j.scitotenv.2020.142456.

Bikkina, S., Andersson, A., Ram, K., Sarin, M.M., Sheesley, R.J., Kirillova, E.N., Rengarajan, R., Sudheer, A.K., Gustafsson, Ö., 2017. Carbon isotope-constrained seasonality of carbonaceous aerosol sources from an urban location (Kanpur) in the Indo-Gangetic Plain. J. Geophys. Res. Atmos. 122, 4903–4923. https://doi.org/10.1002/2016jd025634.

Birch, M.E., Cary, R.A., 1996. Elemental carbon-based method for monitoring occupational exposures to particulate diesel exhaust. Aerosol Sci. Technol. 25, 221–241. https://doi.org/10.1080/02786829608965393.

Bond, T.C., 2001. Spectral dependence of visible light absorption by carbonaceous particles emitted from coal combustion. Geophys. Res. Lett. 28, 4075–4078. https://doi.org/10.1029/2001gl013652.

Bond, T.C., Doherty, S.J., Fahey, D.W., Forster, P.M., Berntsen, T., DeAngelo, B.J., Flanner, M.G., Ghan, S., Kärcher, B., Koch, D., Kinne, S., Kondo, Y., Quinn, P.K., Sarofim, M.C., Schultz, M.G., Schulz, M., Venkataraman, C., Zhang, H., Zhang, S., Bellouin, N., Guttikunda, S.K., Hopke, P.K., Jacobson, M.Z., Kaiser, J.W., Klimont, Z., Lohmann, U., Schwarz, J.P., Shindell, D., Storelvmo, T., Warren, S.G., Zender, C.S., 2013. Bounding the role of black carbon in the climate system: a scientific assessment. J. Geophys. Res. Atmos. 118, 5380–5552. https://doi.org/10.1002/jgrd.50171.

Brown, S.S., Stark, H., Ryerson, T.B., Williams, E.J., Nicks, D.K., Trainer, M., Fehsenfeld, F.C., Ravishankara, A.R., 2003. Nitrogen oxides in the nocturnal boundary layer: simultaneous in situ measurements of NO3, N2O5, NO2, NO, and O3. J. Geophys. Res. Atmos. 108. https://doi.org/10.1029/2002jd002917.

Brown, S.S., Ryerson, T.B., Wollny, A.G., Brock, C.A., Peltier, R., Sullivan, A.P., Weber, R.J., Dube, W.P., Trainer, M., Meagher, J.F., Fehsenfeld, F.C., Ravishankara, A.R., 2006. Variability in nocturnal nitrogen oxide processing and its role in regional air quality. Science 311, 67–70. https://doi.org/10.1126/science.1120120.

Cai, S., Wang, Y., Zhao, B., Wang, S., Chang, X., Hao, J., 2017. The impact of the "Air Pollution Prevention and Control Action Plan" on PM2.5 concentrations in Jing-Jin-Ji region during 2012–2020. Sci. Total Environ. 580, 197–209. https://doi.org/10.1016/j.scitotenv.2016.11.188.

Cai, J., Chu, B.W., Yao, L., Yan, C., Heikkinen, L.M., Zheng, F.X., Li, C., Fan, X.L., Zhang, S.J., Yang, D.Y., Wang, Y.H., Kokkonen, T.V., Chan, T., Zhou, Y., Dada, L., Liu, Y.C., He, H., Paasonen, P., Kujansuu, J.T., Petaja, T., Mohr, C., Kangasluoma, J., Bianchi, F., Sun, Y.L., Croteau, P.L., Worsnop, D.R., Kerminen, V.M., Du, W., Kulmala, M., Daellenbach, K.R., 2020. Size-segregated particle number and mass concentrations from different emission sources in urban Beijing. Atmos. Chem. Phys. 20, 12721–12740. https://doi.org/10.5194/acp-20-12721-2020.

Canonaco, F., Crippa, M., Slowik, J.G., Baltensperger, U., Prévôt, A.S.H., 2013. SoFi, an IGOR-based interface for the efficient use of the generalized multilinear engine (ME-2) for the source apportionment: ME-2 application to aerosol mass spectrometer data. Atmos. Meas. Tech. 6, 3649–3661. https://doi.org/10.5194/amt-6-3649-2013.

Cao, J., Xu, H., Xu, Q., Chen, B., Kan, H., 2012. Fine particulate matter constituents and cardiopulmonary mortality in a heavily polluted Chinese city. Environ. Health Perspect. 120, 373–378. https://doi.org/10.1289/ehp.1103671.

Chen, H., Huo, J., Fu, Q., Duan, Y., Xiao, H., Chen, J., 2020a. Impact of quarantine measures on chemical compositions of PM2.5 during the COVID-19 epidemic in Shanghai, China. Sci. Total Environ. 743, 140758. https://doi.org/10.1016/j.scitotenv.2020.140758.

Chen, Y., Zhang, S., Peng, C., Shi, G., Tian, M., Huang, R.J., Guo, D., Wang, H., Yao, X., Yang, F., 2020b. Impact of the COVID-19 pandemic and control measures on air quality and aerosol light absorption in Southwestern China. Sci. Total Environ. 749, 141419. https://doi.org/10.1016/j.scitotenv.2020.141419.

Chu, B., Dada, L., Liu, Y., Yao, L., Wang, Y., Du, W., Cai, J., Dallenbach, K.R., Chen, X., Simonen, P., Zhou, Y., Deng, C., Fu, Y., Yin, R., Li, H., He, X.C., Feng, Z., Yan, C., Kangasluoma, J., Bianchi, F., Jiang, J., Kujansuu, J., Kerminen, V.M., Petaja, T., He, H., Kulmala, M., 2021. Particle growth with photochemical age from new particle formation to haze in the winter of Beijing,China. Sci. Total Environ. 753, 142207. https://doi.org/10.1016/j.scitotenv.2020.142207.

Countess, R.J., Wolff, G.T., Cadle, S.H., 1980. The Denver winter aerosol: a comprehensive chemical characterization. J. Air Pollut. Control Assoc. 30, 1194–1200. https://doi.org/10.1080/00022470.1980.10465167.

Cui, Y., Ji, D., Maenhaut, W., Gao, W., Zhang, R., Wang, Y., 2020. Levels and sources of hourly PM2.5-related elements during the control period of the COVID-19 pandemic at a rural site between Beijing and Tianjin. Sci. Total Environ. 744, 140840. https://doi.org/10.1016/j.scitotenv.2020.140840.

Daellenbach, K.R., Bozzetti, C., Křepelová, A., Canonaco, F., Wolf, R., Zotter, P., Fermo, P., Crippa, M., Slowik, J.G., Sosedova, Y., Zhang, Y., Huang, R.J., Poulain, L., Szidat, S., Baltensperger, U., El Haddad, I., Prévôt, A.S.H., 2016. Characterization and source apportionment of organic aerosol using offline aerosol mass spectrometry. Atmos. Meas. Tech. 9, 23–39. https://doi.org/10.5194/amt-9-23-2016.

De Gouw, J., Jimenez, J.L., 2009. Organic aerosols in the Earth's atmosphere. Environ. Sci. Technol. 43, 7614–7618. https://doi.org/10.1021/es9006004.

DeCarlo, P.F., Ulbrich, I.M., Crounse, J., de Foy, B., Dunlea, E.J., Aiken, A.C., Knapp, D., Weinheimer, A.J., Campos, T., Wennberg, P.O., Jimenez, J.L., 2010. Investigation of the sources and processing of organic aerosol over the Central Mexican Plateau from aircraft measurements during MILAGRO. Atmos. Chem. Phys. 10, 5257–5280. https://doi.org/10.5194/acp-10-5257-2010.

Dimitriou, K., Kassomenos, P., 2016. Combining AOT, Angstrom exponent and PM concentration data, with PSCF model, to distinguish fine and coarse aerosol intrusions in Southern France. Atmos. Res. 172–173, 74–82. https://doi.org/10.1016/j.atmosres.2016.01.002.

Ding, A.J., Huang, X., Nie, W., Sun, J.N., Kerminen, V.M., Petäjä, T., Su, H., Cheng, Y.F., Yang, X.Q., Wang, M.H., Chi, X.G., Wang, J.P., Virkkula, A., Guo, W.D., Yuan, J., Wang, S.Y., Zhang, R.J., Wu, Y.F., Song, Y., Zhu, T., Zilitinkevich, S., Kulmala, M., Fu, C.B., 2016. Enhanced haze pollution by black carbon in megacities in China. Geophys. Res. Lett. 43, 2873–2879. https://doi.org/10.1002/2016gl067745.

Drinovec, L., Močnik, G., Zotter, P., Prévôt, A.S.H., Ruckstuhl, C., Coz, E., Rupakheti, M., Sciare, J., Müller, T., Wiedensohler, A., Hansen, A.D.A., 2015. The "dual-spot" aethalometer: an improved measurement of aerosol black carbon with real-time loading compensation. Atmos. Meas. Tech. 8, 1965–1979. https://doi.org/10.5194/amt-8-1965-2015.

Fan, C., Li, Z., Li, Y., Dong, J., van der A, R., de Leeuw, G., 2021. Variability of NO2 concentrations over China and effect on air quality derived from satellite and ground-based observations. Atmos. Chem. Phys. 21, 7723–7748. https://doi.org/10.5194/acp-21-7723-2021.

Garg, S., Chandra, B.P., Sinha, V., Sarda-Esteve, R., Gros, V., Sinha, B., 2016. Limitation of the use of the absorption Angstrom exponent for source apportionment of equivalent black carbon: a case study from the North West Indo-Gangetic Plain. Environ. Sci. Technol. 50, 814–824. https://doi.org/10.1021/acs.est.5b03868.

Ge, B., Xu, D., Wild, O., Yao, X., Wang, J., Chen, X., Tan, Q., Pan, X., Wang, Z., 2021. Interannual variations of wet deposition in Beijing from 2014–2017: implications of below-cloud scavenging of inorganic aerosols. Atmos. Chem. Phys. 21, 9441–9454. https://doi.org/10.5194/acp-21-9441-2021.

Harrison, M.A.J., Barra, S., Borghesi, D., Vione, D., Arsene, C., Olariu, R.L., 2005. Nitrated phenols in the atmosphere: a review. Atmos. Environ. 39, 231–248. https://doi.org/10.1016/j.atmosenv.2004.09.044.

Helin, A., Virkkula, A., Backman, J., Pirjola, L., Sippula, O., Aakko-Saksa, P., Väätäinen, S., Mylläri, F., Järvinen, A., Bloss, M., Aurela, M., Jakobi, G., Karjalainen, P., Zimmermann, R., Jokiniemi, J., Saarikoski, S., Tissari, J., Rönkkö, T., Niemi, J.V., Timonen, H., 2021. Variation of absorption Ångström exponent in aerosols from different emission sources. J. Geophys. Res. Atmos. 126. https://doi.org/10.1029/2020jd034094.

Huang, X.F., He, L.Y., Hu, M., Canagaratna, M.R., Sun, Y., Zhang, Q., Zhu, T., Xue, L., Zeng, L.W., Liu, X.G., Zhang, Y.H., Jayne, J.T., Ng, N.L., Worsnop, D.R., 2010. Highly time-resolved chemical characterization of atmospheric submicron particles during 2008 Beijing Olympic Games using an Aerodyne High-resolution Aerosol Mass Spectrometer. Atmos. Chem. Phys. 10, 8933–8945. https://doi.org/10.5194/acp-10-8933-2010.

Huang, K., Zhang, X., Lin, Y., 2015. The "APEC Blue" phenomenon: regional emission control effects observed from space. Atmos. Res. 164–165, 65–75. https://doi.org/10.1016/j.atmosres.2015.04.018.

Huang, X., Ding, A., Gao, J., Zheng, B., Zhou, D., Qi, X., Tang, R., Wang, J., Ren, C., Nie, W., Chi, X., Xu, Z., Chen, L., Li, Y., Che, F., Pang, N., Wang, H., Tong, D., Qin, W., Cheng, W., Liu, W., Fu, Q., Liu, B., Chai, F., Davis, S.J., Zhang, Q., He, K., 2021. Enhanced secondary pollution offset reduction of primary emissions during COVID-19 lockdown in China. Natl. Sci. Rev. 8. https://doi.org/10.1093/nsr/nwaa137.

Japar, S.M., Szkarlat, A.C., Gorse, R.A., Heyerdahl, E.K., Johnson, R.L., Rau, J.A., Huntzicker, J.J., 1984. Comparison of solvent extraction and thermal-optical carbon analysis methods: application to diesel vehicle exhaust aerosol. Environ. Sci. Technol. 18, 231–234. https://doi.org/10.1021/es00122a004.

Ji, D., Yan, Y., Wang, Z., He, J., Liu, B., Sun, Y., Gao, M., Li, Y., Cao, W., Cui, Y., Hu, B., Xin, J., Wang, L., Liu, Z., Tang, G., Wang, Y., 2018a. Two-year continuous measurements of carbonaceous aerosols in urban Beijing, China: temporal variations, characteristics and source analyses. Chemosphere 200, 191–200. https://doi.org/10.1016/j.chemosphere.2018.02.067.

Ji, Y., Qin, X., Wang, B., Xu, J., Shen, J., Chen, J., Huang, K., Deng, C., Yan, R., Xu, K., Zhang, T., 2018b. Counteractive effects of regional transport and emission control on the formation of fine particles: a case study during the Hangzhou G20 summit. Atmos. Chem. Phys. 18, 13581–13600. https://doi.org/10.5194/acp-18-13581-2018.

Jing, A., Zhu, B., Wang, H., Yu, X., An, J., Kang, H., 2019. Source apportionment of black carbon in different seasons in the northern suburb of Nanjing,China. Atmos. Environ. 201, 190–200. https://doi.org/10.1016/j.atmosenv.2018.12.060.

Jokinen, T., Sipilä, M., Junninen, H., Ehn, M., Lönn, G., Hakala, J., Petäjä, T., Mauldin, R.L., Kulmala, M., Worsnop, D.R., 2012. Atmospheric sulphuric acid and neutral cluster measurements using CI-APi-TOF. Atmos. Chem. Phys. 12, 4117–4125. https://doi.org/10.5194/acp-12-4117-2012.

Junninen, H., Ehn, M., Petäjä, T., Luosujärvi, L., Kotiaho, T., Kostiainen, R., Rohner, U., Gonin, M., Fuhrer, K., Kulmala, M., Worsnop, D.R., 2010. A high-resolution mass spectrometer to measure atmospheric ion composition. Atmos. Meas. Tech. 3, 1039–1053. https://doi.org/10.5194/amt-3-1039-2010.

Kang, M., Zhang, J., Zhang, H., Ying, Q., 2021. On the relevancy of observed ozone increase during COVID-19 lockdown to summertime ozone and PM2.5 control policies in China. Environ. Sci. Technol. Lett. 8, 289–294. https://doi.org/10.1021/acs.estlett.1c00036.

Kanniah, K.D., Kamarul Zaman, N.A.F., Kaskaoutis, D.G., Latif, M.T., 2020. COVID-19's impact on the atmospheric environment in the Southeast Asia region. Sci. Total Environ. 736. https://doi.org/10.1016/j.scitotenv.2020.139658.

Kercher, J.P., Riedel, T.P., Thornton, J.A., 2009. Chlorine activation by N2O5: simultaneous, in situ detection of ClNO2 and N2O5 by chemical ionization mass spectrometry. Atmos. Meas. Tech. 2, 193–204. https://doi.org/10.5194/amt-2-193-2009.

Kirchstetter, T.W., Novakov, T., Hobbs, P.V., 2004. Evidence that the spectral dependence of light absorption by aerosols is affected by organic carbon. J. Geophys. Res. Atmos. 109. https://doi.org/10.1029/2004jd004999.

Kley, D., Geiss, H., Mohnen, V.A., 1994. Tropospheric ozone at elevated sites and precursor emissions in the United States and Europe. Atmos. Environ. 28, 149–158. https://doi.org/10.1016/1352-2310(94)90030-2.

Klingshirn, C.D., West, Z.J., DeWitt, M.J., Higgins, A., Graham, J., Corporan, E., 2019. Quantification of elemental and total carbon in combustion particulate matter using thermal-oxidative analysis. J. Air Waste Manag. Assoc. 69, 1003–1013. https://doi.org/10.1080/10962247.2019.1630025.

Kuang, Y., He, Y., Xu, W., Yuan, B., Zhang, G., Ma, Z., Wu, C., Wang, C., Wang, S., Zhang, S., Tao, J., Ma, N., Su, H., Cheng, Y., Shao, M., Sun, Y., 2020. Photochemical aqueous-phase reactions induce rapid daytime formation of oxygenated organic aerosol on the North China Plain. Environ. Sci. Technol. 54, 3849–3860. https://doi.org/10.1021/acs.est.9b06836.

Kurtén, T., Petäjä, T., Smith, J., Ortega, I.K., Sipilä, M., Junninen, H., Ehn, M., Vehkamäki, H., Mauldin, L., Worsnop, D.R., Kulmala, M., 2011. The effect of H2SO4 – amine clustering on chemical ionization mass spectrometry (CIMS) measurements of gas-phase sulfuric acid. Atmos. Chem. Phys. 11, 3007–3019. https://doi.org/10.5194/acp-11-3007-2011.

Lack, D.A., Langridge, J.M., 2013. On the attribution of black and brown carbon light absorption using the Ångström exponent. Atmos. Chem. Phys. 13, 10535–10543. https://doi.org/10.5194/acp-13-10535-2013.

Laskin, A., Laskin, J., Nizkorodov, S.A., 2015. Chemistry of atmospheric brown carbon. Chem. Rev. 115, 4335–4382. https://doi.org/10.1021/cr5006167.

Le, T., Wang, Y., Liu, L., Yang, J., Yung, Y.L., Li, G., Seinfeld, J.H., 2020. Unexpected air pollution with marked emission reductions during the COVID-19 outbreak in China. Science 369, 702–706. https://doi.org/10.1126/science.abb7431.

Lee, J.D., Drysdale, W.S., Finch, D.P., Wilde, S.E., Palmer, P.I., 2020. UK surface NO2 levels dropped by 42 % during the COVID-19 lockdown: impact on surface O3. Atmos. Chem. Phys. 20, 15743–15759. https://doi.org/10.5194/acp-20-15743-2020.

Leighton, P., 2012. Photochemistry of Air Pollution. Elsevier.

Li, X., Wang, S., Duan, L., Hao, J., Nie, Y., 2009. Carbonaceous aerosol emissions from household biofuel combustion in China. Environ. Sci. Technol. 43, 6076–6081. https://doi.org/10.1021/es803330j.

Li, K., Chen, L., White, S.J., Zheng, X., Lv, B., Lin, C., Bao, Z., Wu, X., Gao, X., Ying, F., Shen, J., Azzi, M., Cen, K., 2018. Chemical characteristics and sources of PM1 during the 2016 summer in Hangzhou. Environ. Pollut. 232, 42–54. https://doi.org/10.1016/j.envpol.2017.09.016.

Li, J., Han, Z., Wu, Y., Xiong, Z., Xia, X., Li, J., Liang, L., Zhang, R., 2020. Aerosol radiative effects and feedbacks on boundary layer meteorology and PM2.5 chemical components during winter haze events over the Beijing-Tianjin-Hebei region. Atmos. Chem. Phys. 20, 8659–8690. https://doi.org/10.5194/acp-20-8659-2020.

Li, K., Jacob, D.J., Liao, H., Qiu, Y., Shen, L., Zhai, S., Bates, K.H., Sulprizio, M.P., Song, S., Lu, X., Zhang, Q., Zheng, B., Zhang, Y., Zhang, J., Lee, H.C., Kuk, S.K., 2021a. Ozone pollution in the North China Plain spreading into the late-winter haze season. Proc. Natl. Acad. Sci. 118. https://doi.org/10.1073/pnas.2015797118.

Li, X., Bei, N., Hu, B., Wu, J., Pan, Y., Wen, T., Liu, Z., Liu, L., Wang, R., Li, G., 2021b. Mitigating NOX emissions does not help alleviate wintertime particulate pollution in Beijing-Tianjin-Hebei,China. Environ. Pollut. 279, 116931. https://doi.org/10.1016/j.envpol.2021.116931.

Liakakou, E., Kaskaoutis, D.G., Grivas, G., Stavroulas, I., Tsagkaraki, M., Paraskevopoulou, D., Bougiatioti, A., Dumka, U.C., Gerasopoulos, E., Mihalopoulos, N., 2020. Long-term brown carbon spectral characteristics in a Mediterranean city (Athens). Sci. Total Environ. 708, 135019. https://doi.org/10.1016/j.scitotenv.2019.135019.

Lin, Y.-C., Zhang, Y.-L., Xie, F., Fan, M.-Y., Liu, X., 2021. Substantial decreases of light absorption, concentrations and relative contributions of fossil fuel to light-absorbing carbonaceous aerosols attributed to the COVID-19 lockdown in east China. Environ. Pollut. 275. https://doi.org/10.1016/j.envpol.2021.116615.

Liu, C., Chung, C.E., Yin, Y., Schnaiter, M., 2018. The absorption Ångström exponent of black carbon: from numerical aspects. Atmos. Chem. Phys. 18, 6259–6273. https://doi.org/10.5194/acp-18-6259-2018.

Liu, J., Zheng, Y., Geng, G., Hong, C., Li, M., Li, X., Liu, F., Tong, D., Wu, R., Zheng, B., He, K., Zhang, Q., 2020a. Decadal changes in anthropogenic source contribution of PM2.5 pollution and related health impacts in China, 1990–2015. Atmos. Chem. Phys. 20, 7783–7799. https://doi.org/10.5194/acp-20-7783-2020.

Liu, Y., Ni, S., Jiang, T., Xing, S., Zhang, Y., Bao, X., Feng, Z., Fan, X., Zhang, L., Feng, H., 2020b. Influence of Chinese New Year overlapping COVID-19 lockdown on HONO sources in Shijiazhuang. Sci. Total Environ. 745, 141025. https://doi.org/10.1016/j.scitotenv.2020.141025.

Liu, Y., Yan, C., Feng, Z., Zheng, F., Fan, X., Zhang, Y., Li, C., Zhou, Y., Lin, Z., Guo, Y., Zhang, Y., Ma, L., Zhou, W., Liu, Z., Dada, L., Dällenbach, K., Kontkanen, J., Cai, R., Chan, T., Chu, B., Du, W., Yao, L., Wang, Y., Cai, J., Kangasluoma, J., Kokkonen, T., Kujansuu, J., Rusanen, A., Deng, C., Fu, Y., Yin, R., Li, X., Lu, Y., Liu, Y., Lian, C., Yang, D., Wang, W., Ge, M., Wang, Y., Worsnop, D.R., Junninen, H., He, H., Kerminen, V.-M., Zheng, J., Wang, L., Jiang, J., Petäjä, T., Bianchi, F., Kulmala, M., 2020c. Continuous and comprehensive atmospheric observations in Beijing: a station to understand the complex urban atmospheric environment. Big Earth Data 4, 295–321. https://doi.org/10.1080/20964471.2020.1798707.

Lopez-Hilfiker, F.D., Mohr, C., Ehn, M., Rubach, F., Kleist, E., Wildt, J., Mentel, T.F., Lutz, A., Hallquist, M., Worsnop, D., Thornton, J.A., 2014. A novel method for online analysis of gas and particle composition: description and evaluation of a Filter Inlet for Gases and AEROsols (FIGAERO). Atmos. Meas. Tech. 7, 983–1001. https://doi.org/10.5194/amt-7-983-2014.

Lu, D., Zhang, J., Xue, C., Zuo, P., Chen, Z., Zhang, L., Ling, W., Liu, Q., Jiang, G., 2021. COVID-19-induced lockdowns indicate the short-term control effect of air pollutant emission in 174 cities in China. Environ. Sci. Technol. 55, 4094–4102. https://doi.org/10.1021/acs.est.0c07170.

Ma, Y., Fu, T.-M., Tian, H., Gao, J., Hu, M., Guo, J., Zhang, Y., Sun, Y., Zhang, L., Yang, X., Wang, X., 2020. Emergency response measures to alleviate a severe haze pollution event in northern China during December 2015: assessment of effectiveness. Aerosol Air Qual. Res. 20, 2098–2116. https://doi.org/10.4209/aaqr.2019.09.0442.

Ma, J., Shen, J., Wang, P., Zhu, S., Wang, Y., Wang, P., Wang, G., Chen, J., Zhang, H., 2021. Modeled changes in source contributions of particulate matter during the COVID-19 pandemic in the Yangtze River Delta,China. Atmos. Chem. Phys. 21, 7343–7355. https://doi.org/10.5194/acp-21-7343-2021.

Meng, R., Zhao, F., Sun, K., Zhang, R., Huang, C., Yang, J., 2015. Analysis of the 2014 "APEC Blue" in Beijing using more than one decade of satellite observations: lessons learned from radical emission control measures. Remote Sens. 7, 15224–15243. https://doi.org/10.3390/rs71115224.

Metya, A., Dagupta, P., Halder, S., Chakraborty, S., Tiwari, Y.K., 2020. COVID-19 lockdowns improve air quality in the south-east Asian regions, as seen by the remote sensing satellites. Aerosol Air Qual. Res. 20, 1772–1782. https://doi.org/10.4209/aaqr.2020.05.0240.

Middlebrook, A.M., Bahreini, R., Jimenez, J.L., Canagaratna, M.R., 2012. Evaluation of composition-dependent collection efficiencies for the aerodyne aerosol mass spectrometer using field data. Aerosol Sci. Technol. 46, 258–271. https://doi.org/10.1080/02786826.2011.620041.

Millet, D.B., Donahue, N.M., Pandis, S.N., Polidori, A., Stanier, C.O., Turpin, B.J., Goldstein, A.H., 2005. Atmospheric volatile organic compound measurements during the Pittsburgh Air Quality Study: results, interpretation, and quantification of primary and secondary contributions. J. Geophys. Res. Atmos. 110. https://doi.org/10.1029/2004jd004601.

Nichol, J.E., Bilal, M., Ali, M.A., Qiu, Z., 2020. Air pollution scenario over China during COVID-19. Remote Sens. 12. https://doi.org/10.3390/rs12132100.

Notario, A., Bravo, I., Adame, J.A., Díaz-de-Mera, Y., Aranda, A., Rodríguez, A., Rodríguez, D., 2013. Variability of oxidants (OX = O3 + NO2), and preliminary study on ambient levels of ultrafine particles and VOCs, in an important ecological area in Spain. Atmos. Res. 128, 35–45. https://doi.org/10.1016/j.atmosres.2013.03.008.

Otmani, A., Benchrif, A., Tahri, M., Bounakhla, M., Chakir, E.M., El Bouch, M., Krombi, M., 2020. Impact of Covid-19 lockdown on PM10, SO2 and NO2 concentrations in Sale City (Morocco). Sci. Total Environ. 735, 139541. https://doi.org/10.1016/j.scitotenv.2020.139541.

Polissar, A., 1999. The aerosol at Barrow, Alaska: long-term trends and source locations. Atmos. Environ. 33, 2441–2458. https://doi.org/10.1016/s1352-2310(98)00423-3.

Ram, K., Sarin, M.M., Hegde, P., 2008. Atmospheric abundances of primary and secondary carbonaceous species at two high-altitude sites in India: sources and temporal variability. Atmos. Environ. 42, 6785–6796. https://doi.org/10.1016/j.atmosenv.2008.05.031.

Rattigan, O.V., Dirk Felton, H., Bae, M.-S., Schwab, J.J., Demerjian, K.L., 2010. Multi-year hourly PM2.5 carbon measurements in New York: diurnal, day of week and seasonal patterns. Atmos. Environ. 44, 2043–2053. https://doi.org/10.1016/j.atmosenv.2010.01.019.

Ren, Y., Li, H., Meng, F., Wang, G., Zhang, H., Yang, T., Li, W., Ji, Y., Bi, F., Wang, X., 2019. Impact of emission controls on air quality in Beijing during the 2015 China Victory Day Parade: implication from organic aerosols. Atmos. Environ. 198, 207–214. https://doi.org/10.1016/j.atmosenv.2018.10.061.

Ren, Y.Q., Wei, J., Ji, Y.Y., Wu, Z.H., Bi, F., Gao, R., Wang, X.Z., Li, H., 2021. Chemical composition of fine organic aerosols during a moderate pollution event in summertime in Beijing: combined effect of primary emission and secondary formation. Atmos. Environ. 246. https://doi.org/10.1016/j.atmosenv.2020.118167.

Safai, P.D., Raju, M.P., Rao, P.S.P., Pandithurai, G., 2014. Characterization of carbonaceous aerosols over the urban tropical location and a new approach to evaluate their climatic importance. Atmos. Environ. 92, 493–500. https://doi.org/10.1016/j.atmosenv.2014.04.055.

Sosa, B.S., Porta, A., Colman Lerner, J.E., Banda Noriega, R., Massolo, L., 2017. Human health risk due to variations in PM 10 -PM 2.5 and associated PAHs levels. Atmos. Environ. 160, 27–35. https://doi.org/10.1016/j.atmosenv.2017.04.004.

Sun, Y., Wang, Z., Wild, O., Xu, W., Chen, C., Fu, P., Du, W., Zhou, L., Zhang, Q., Han, T., Wang, Q., Pan, X., Zheng, H., Li, J., Guo, X., Liu, J., Worsnop, D.R., 2016. "APEC Blue": secondary aerosol reductions from emission controls in Beijing. Sci. Rep. 6, 20668. https://doi.org/10.1038/srep20668.

Sun, T., Che, H., Qi, B., Wang, Y., Dong, Y., Xia, X., Wang, H., Gui, K., Zheng, Y., Zhao, H., Ma, Q., Du, R., Zhang, X., 2019a. Characterization of vertical distribution and radiative forcing of ambient aerosol over the Yangtze River Delta during 2013–2015. Sci. Total Environ. 650, 1846–1857. https://doi.org/10.1016/j.scitotenv.2018.09.262.

Sun, W., Wang, D., Yao, L., Fu, H., Fu, Q., Wang, H., Li, Q., Wang, L., Yang, X., Xian, A., Wang, G., Xiao, H., Chen, J., 2019b. Chemistry-triggered events of PM2.5 explosive growth during late autumn and winter in Shanghai,China. Environ. Pollut. 254, 112864. https://doi.org/10.1016/j.envpol.2019.07.032.

Sun, J.Y., Wu, C., Wu, D., Cheng, C., Li, M., Li, L., Deng, T., Yu, J.Z., Li, Y.J., Zhou, Q., Liang, Y., Sun, T., Song, L., Cheng, P., Yang, W., Pei, C., Chen, Y., Cen, Y., Nian, H., Zhou, Z., 2020a. Amplification of black carbon light absorption induced by atmospheric aging: temporal variation at seasonal and diel scales in urban Guangzhou. Atmos. Chem. Phys. 20, 2445–2470. https://doi.org/10.5194/acp-20-2445-2020.

Sun, Y., Lei, L., Zhou, W., Chen, C., He, Y., Sun, J., Li, Z., Xu, W., Wang, Q., Ji, D., Fu, P., Wang, Z., Worsnop, D.R., 2020b. A chemical cocktail during the COVID-19 outbreak in Beijing, China: insights from six-year aerosol particle composition measurements during the Chinese New Year holiday. Sci. Total Environ. 742, 140739. https://doi.org/10.1016/j.scitotenv.2020.140739.

Sun, J., Xie, C., Xu, W., Chen, C., Ma, N., Xu, W., Lei, L., Li, Z., He, Y., Qiu, Y., Wang, Q., Pan, X., Su, H., Cheng, Y., Wu, C., Fu, P., Wang, Z., Sun, Y., 2021a. Light absorption of black carbon and brown carbon in winter in North China Plain: comparisons between urban and rural sites. Sci. Total Environ. 770, 144821. https://doi.org/10.1016/j.scitotenv.2020.144821.

Sun, Z., Zhao, X., Li, Z., Tang, G., Miao, S., 2021b. Boundary layer structure characteristics under objective classification of persistent pollution weather types in the Beijing area. Atmos. Chem. Phys. 21, 8863–8882. https://doi.org/10.5194/acp-21-8863-2021.

Tao, J., Zhang, L., Cao, J., Zhang, R., 2017. A review of current knowledge concerning PM2.5 chemical composition, aerosol optical properties and their relationships across China. Atmos. Chem. Phys. 17, 9485–9518. https://doi.org/10.5194/acp-17-9485-2017.

Turpin, B.J., Huntzicker, J.J., 1995. Identification of secondary organic aerosol episodes and quantitation of primary and secondary organic aerosol concentrations during SCAQS. Atmos. Environ. 29, 3527–3544. https://doi.org/10.1016/1352-2310(94)00276-q.

Virkkula, A., Chi, X., Ding, A., Shen, Y., Nie, W., Qi, X., Zheng, L., Huang, X., Xie, Y., Wang, J., Petäjä, T., Kulmala, M., 2015. On the interpretation of the loading correction of the aethalometer. Atmos. Meas. Tech. 8, 4415–4427. https://doi.org/10.5194/amt-8-4415-2015.

Wang, Y.Q., 2014. MeteoInfo: GIS software for meteorological data visualization and analysis. Meteorol. Appl. 21, 360–368. https://doi.org/10.1002/met.13.

Wang, Y.Q., 2019. An open source software suite for multi-dimensional meteorological data computation and visualisation. J. Open Res. Softw. 7. https://doi.org/10.5334/jors.267.

Wang, Y.Q., Zhang, X.Y., Draxler, R.R., 2009. TrajStat: GIS-based software that uses various trajectory statistical analysis methods to identify potential sources from long-term air pollution measurement data. Environ. Model. Softw. 24, 938–939. https://doi.org/10.1016/j.envsoft.2009.01.004.

Wang, S., Zhao, M., Xing, J., Wu, Y., Zhou, Y., Lei, Y., He, K., Fu, L., Hao, J., 2010. Quantifying the air pollutants emission reduction during the 2008 Olympic games in Beijing. Environ. Sci. Technol. 44, 2490–2496. https://doi.org/10.1021/es9028167.

Wang, Y., Yao, L., Wang, L., Liu, Z., Ji, D., Tang, G., Zhang, J., Sun, Y., Hu, B., Xin, J., 2013. Mechanism for the formation of the January 2013 heavy haze pollution episode over central and eastern China. Sci. China: Earth Sci. 57, 14–25. https://doi.org/10.1007/s11430-013-4773-4.

Wang, T., Tham, Y.J., Xue, L., Li, Q., Zha, Q., Wang, Z., Poon, S.C., Dubé, W.P., Blake, D.R., Louie, P.K., 2016. Observations of nitryl chloride and modeling its source and effect on ozone in the planetary boundary layer of southern China. J. Geophys. Res. Atmos. 121, 2476–2489. https://doi.org/10.1002/2015JD024556.

Wang, J., Zhao, B., Wang, S., Yang, F., Xing, J., Morawska, L., Ding, A., Kulmala, M., Kerminen, V.M., Kujansuu, J., Wang, Z., Ding, D., Zhang, X., Wang, H., Tian, M., Petaja, T., Jiang, J., Hao, J., 2017. Particulate matter pollution over China and the effects of control policies. Sci. Total Environ. 584–585, 426–447. https://doi.org/10.1016/j.scitotenv.2017.01.027.

Wang, L., Schlagal, C.R., Gao, J., Hao, Y., Dunn, T.J., McGrath, E.L., Labastida, J.A., Yu, Y., Feng, S.Q., Liu, S.Y., Wu, P., 2018. Oligodendrocyte differentiation from human neural stem cells: a novel role for c-Src. Neurochem. Int. 120, 21–32. https://doi.org/10.1016/j.neuint.2018.07.006.

Wang, Q., Ye, J., Wang, Y., Zhang, T., Ran, W., Wu, Y., Tian, J., Li, L., Zhou, Y., Hang Ho, S.S., Dang, B., Zhang, Q., Zhang, R., Chen, Y., Zhu, C., Cao, J., 2019. Wintertime optical properties of primary and secondary brown carbon at a regional site in the North China Plain. Environ. Sci. Technol. 53, 12389–12397. https://doi.org/10.1021/acs.est.9b03406.

Wang, P., Chen, K., Zhu, S., Wang, P., Zhang, H., 2020a. Severe air pollution events not avoided by reduced anthropogenic activities during COVID-19 outbreak. Resour. Conserv. Recycl. 158, 104814. https://doi.org/10.1016/j.resconrec.2020.104814.

Wang, Q., Liu, H., Wang, P., Dai, W., Zhang, T., Zhao, Y., Tian, J., Zhang, W., Han, Y., Cao, J., 2020b. Optical source apportionment and radiative effect of light-absorbing carbonaceous aerosols in a tropical marine monsoon climate zone: the importance of ship emissions. Atmos. Chem. Phys. 20, 15537–15549. https://doi.org/10.5194/acp-20-15537-2020.

Wang, Q., Liu, H., Ye, J., Tian, J., Zhang, T., Zhang, Y., Liu, S., Cao, J., 2020c. Estimating absorption Ångström exponent of black carbon aerosol by coupling multiwavelength absorption with chemical composition. Environ. Sci. Technol. Lett. 8, 121–127. https://doi.org/10.1021/acs.estlett.0c00829.

Wang, Y., Gao, W., Wang, S., Song, T., Gong, Z., Ji, D., Wang, L., Liu, Z., Tang, G., Huo, Y., Tian, S., Li, J., Li, M., Yang, Y., Chu, B., Petäjä, T., Kerminen, V.-M., He, H., Hao, J., Kulmala, M., Wang, Y., Zhang, Y., 2020d. Contrasting trends of PM2.5 and surface-ozone concentrations in China from 2013 to 2017. Natl. Sci. Rev. 7, 1331–1339. https://doi.org/10.1093/nsr/nwaa032.

Wang, Y., Hu, M., Xu, N., Qin, Y., Wu, Z., Zeng, L., Huang, X., He, L., 2020e. Chemical composition and light absorption of carbonaceous aerosols emitted from crop residue burning: influence of combustion efficiency. Atmos. Chem. Phys. 20, 13721–13734. https://doi.org/10.5194/acp-20-13721-2020.

Wang, J., Lei, Y., Chen, Y., Wu, Y., Ge, X., Shen, F., Zhang, J., Ye, J., Nie, D., Zhao, X., Chen, M., 2021a. Comparison of air pollutants and their health effects in two developed regions in China during the COVID-19 pandemic. J. Environ. Manag. 287, 112296. https://doi.org/10.1016/j.jenvman.2021.112296.

Wang, K., Huang, R.-J., Brüggemann, M., Zhang, Y., Yang, L., Ni, H., Guo, J., Wang, M., Han, J., Bilde, M., Glasius, M., Hoffmann, T., 2021b. Urban organic aerosol composition in eastern China differs from north to south: molecular insight from a liquid chromatography–mass spectrometry (Orbitrap) study. Atmos. Chem. Phys. 21, 9089–9104. https://doi.org/10.5194/acp-21-9089-2021.

Watson, J.G., 2002. Visibility: science and regulation. J. Air Waste Manag. Assoc. 52, 628–713. https://doi.org/10.1080/10473289.2002.10470813.

Wu, C., Yu, J.Z., 2016. Determination of primary combustion source organic carbon-to-elemental carbon (OC/EC) ratio using ambient OC and EC measurements: secondary OC-EC correlation minimization method. Atmos. Chem. Phys. 16, 5453–5465. https://doi.org/10.5194/acp-16-5453-2016.

Wu, C., Wu, D., Yu, J.Z., 2019. Estimation and uncertainty analysis of secondary organic carbon using 1 year of hourly organic and elemental carbon data. J. Geophys. Res. Atmos. 124, 2774–2795. https://doi.org/10.1029/2018jd029290.

Xie, Y., Liu, Z., Wen, T., Huang, X., Liu, J., Tang, G., Yang, Y., Li, X., Shen, R., Hu, B., Wang, Y., 2019. Characteristics of chemical composition and seasonal variations of PM2.5 in Shijiazhuang, China: impact of primary emissions and secondary formation. Sci. Total Environ. 677, 215–229. https://doi.org/10.1016/j.scitotenv.2019.04.300.

Xing, L., Fu, T.M., Cao, J.J., Lee, S.C., Wang, G.H., Ho, K.F., Cheng, M.C., You, C.F., Wang, T.J., 2013. Seasonal and spatial variability of the OM/OC mass ratios and high regional correlation between oxalic acid and zinc in Chinese urban organic aerosols. Atmos. Chem. Phys. 13, 4307–4318. https://doi.org/10.5194/acp-13-4307-2013.

Yao, L., Huo, J., Wang, D., Fu, Q., Sun, W., Li, Q., Chen, J., 2020. Online measurement of carbonaceous aerosols in suburban Shanghai during winter over a three-year period: temporal variations, meteorological effects, and sources. Atmos. Environ. 226. https://doi.org/10.1016/j.atmosenv.2020.117408.

Zhang, R., Jing, J., Tao, J., Hsu, S.C., Wang, G., Cao, J., Lee, C.S.L., Zhu, L., Chen, Z., Zhao, Y., Shen, Z., 2013a. Chemical characterization and source apportionment of PM2.5 in Beijing: seasonal perspective. Atmos. Chem. Phys. 13, 7053–7074. https://doi.org/10.5194/acp-13-7053-2013.

Zhang, X., Lin, Y.H., Surratt, J.D., Weber, R.J., 2013b. Sources, composition and absorption Angstrom exponent of light-absorbing organic components in aerosol extracts from the Los Angeles Basin. Environ. Sci. Technol. 47, 3685–3693. https://doi.org/10.1021/es305047b.

Zhang, Q., Sarkar, S., Wang, X., Zhang, J., Mao, J., Yang, L., Shi, Y., Jia, S., 2019a. Evaluation of factors influencing secondary organic carbon (SOC) estimation by CO and EC tracer methods. Sci. Total Environ. 686, 915–930. https://doi.org/10.1016/j.scitotenv.2019.05.402.

Zhang, Q., Zheng, Y., Tong, D., Shao, M., Wang, S., Zhang, Y., Xu, X., Wang, J., He, H., Liu, W., Ding, Y., Lei, Y., Li, J., Wang, Z., Zhang, X., Wang, Y., Cheng, J., Liu, Y., Shi, Q., Yan, L., Geng, G., Hong, C., Li, M., Liu, F., Zheng, B., Cao, J., Ding, A., Gao, J., Fu, Q., Huo, J., Liu, B., Liu, Z., Yang, F., He, K., Hao, J., 2019b. Drivers of improved PM2.5 air quality in

China from 2013 to 2017. Proc. Natl. Acad. Sci. 116, 24463–24469. https://doi.org/10.1073/pnas.1907956116.

Zhang, M., Katiyar, A., Zhu, S., Shen, J., Xia, M., Ma, J., Kota, S.H., Wang, P., Zhang, H., 2021a. Impact of reduced anthropogenic emissions during COVID-19 on air quality in India. Atmos. Chem. Phys. 21, 4025–4037. https://doi.org/10.5194/acp-21-4025-2021.

Zhang, W., Wang, W., Li, J., Ma, S., Lian, C., Li, K., Shi, B., Liu, M., Li, Y., Wang, Q., Sun, Y., Tong, S., Ge, M., 2021b. Light absorption properties and potential sources of brown carbon in Fenwei Plain during winter 2018–2019. J. Environ. Sci. 102, 53–63. https://doi.org/10.1016/j.jes.2020.09.007.

Zhao, P.S., Dong, F., He, D., Zhao, X.J., Zhang, X.L., Zhang, W.Z., Yao, Q., Liu, H.Y., 2013. Characteristics of concentrations and chemical compositions for PM2.5 in the region of Beijing, Tianjin, and Hebei,China. Atmos. Chem. Phys. 13, 4631–4644. https://doi.org/10.5194/acp-13-4631-2013.

Zhao, J., Du, W., Zhang, Y., Wang, Q., Chen, C., Xu, W., Han, T., Wang, Y., Fu, P., Wang, Z., Li, Z., Sun, Y., 2017. Insights into aerosol chemistry during the 2015 China Victory Day parade: results from simultaneous measurements at ground level and 260 m in Beijing. Atmos. Chem. Phys. 17, 3215–3232. https://doi.org/10.5194/acp-17-3215-2017.

Zhao, N., Wang, G., Li, G., Lang, J., Zhang, H., 2020. Air pollution episodes during the COVID-19 outbreak in the Beijing–Tianjin–Hebei region of China: an insight into the transport pathways and source distribution. Environ. Pollut. 267. https://doi.org/10.1016/j.envpol.2020.115617.

Zheng, G.J., Duan, F.K., Su, H., Ma, Y.L., Cheng, Y., Zheng, B., Zhang, Q., Huang, T., Kimoto, T., Chang, D., Pöschl, U., Cheng, Y.F., He, K.B., 2015. Exploring the severe winter haze in Beijing: the impact of synoptic weather, regional transport and heterogeneous reactions. Atmos. Chem. Phys. 15, 2969–2983. https://doi.org/10.5194/acp-15-2969-2015.

Zheng, H., Kong, S., Chen, N., Yan, Y., Liu, D., Zhu, B., Xu, K., Cao, W., Ding, Q., Lan, B., Zhang, Z., Zheng, M., Fan, Z., Cheng, Y., Zheng, S., Yao, L., Bai, Y., Zhao, T., Qi, S., 2020. Significant changes in the chemical compositions and sources of PM2.5 in Wuhan since the city lockdown as COVID-19. Sci. Total Environ. 739, 140000. https://doi.org/10.1016/j.scitotenv.2020.140000.

Zhong, J., Zhang, X., Dong, Y., Wang, Y., Liu, C., Wang, J., Zhang, Y., Che, H., 2018. Feedback effects of boundary-layer meteorological factors on cumulative explosive growth of PM2.5; during winter heavy pollution episodes in Beijing from 2013 to 2016. Atmos. Chem. Phys. 18, 247–258. https://doi.org/10.5194/acp-18-247-2018.

Zhou, Y., Dada, L., Liu, Y., Fu, Y., Kangasluoma, J., Chan, T., Yan, C., Chu, B., Daellenbach, K.R., Bianchi, F., Kokkonen, T., Liu, Y., Kujansuu, J., Kerminen, V.-M., Petäjä, T., Wang, L., Jiang, J., Kulmala, M., 2019. Variation of size-segregated particle number concentrations in winter Beijing. Atmos. Chem. Phys. 1–31. https://doi.org/10.5194/acp-2019-60.

Zong, Z., Wang, X., Tian, C., Chen, Y., Fu, S., Qu, L., Ji, L., Li, J., Zhang, G., 2018. PMF and PSCF based source apportionment of PM2.5 at a regional background site in North China. Atmos. Res. 203, 207–215. https://doi.org/10.1016/j.atmosres.2017.12.013.

Zong, L., Yang, Y., Gao, M., Wang, H., Wang, P., Zhang, H., Wang, L., Ning, G., Liu, C., Li, Y., Gao, Z., 2021. Large-scale synoptic drivers of co-occurring summertime ozone and PM2.5 pollution in eastern China. Atmos. Chem. Phys. 21, 9105–9124. https://doi.org/10.5194/acp-21-9105-2021.

Zoran, M.A., Savastru, R.S., Savastru, D.M., Tautan, M.N., 2020. Assessing the relationship between surface levels of PM2.5 and PM10 particulate matter impact on COVID-19 in Milan, Italy. Sci. Total Environ. 738, 139825. https://doi.org/10.1016/j.scitotenv.2020.139825.